

The influence of metallicity on the Leavitt Law from geometrical distances of Milky Way and Magellanic Clouds Cepheids

LOUISE BREUVAL,¹ PIERRE KERVELLA,¹ PIOTR WIELGÓRSKI,² WOLFGANG GIEREN,³ DARIUSZ GRACZYK,⁴ BORIS TRAHIN,¹
GRZEGORZ PIETRZYŃSKI,² FRÉDÉRIC ARENOU,⁵ BEHNAM JAVANMARDI,¹ AND BARTŁOMIEJ ZGIRSKI²

¹*LESIA, Observatoire de Paris, Université PSL, CNRS, Sorbonne Université, Université de Paris, 5 place Jules Janssen, 92195 Meudon, France*

²*Nicolaus Copernicus Astronomical Centre, Polish Academy of Sciences, Bartycka 18, 00-716 Warszawa, Poland*

³*Universidad de Concepción, Departamento de Astronomía, Casilla 160-C, Concepción, Chile*

⁴*Centrum Astronomiczne im. Mikołaja Kopernika, Polish Academy of Sciences, Rabiańska 8, 87-100, Toruń, Poland*

⁵*GEPI, Observatoire de Paris, Université PSL, CNRS, 5 place Jules Janssen, 92190 Meudon, France*

(Received 29 January 2021; Revised 12 March 2021; Accepted 18 March 2021)

Submitted to ApJ

ABSTRACT

The Cepheid Period-Luminosity (PL) relation is the key tool for measuring astronomical distances and for establishing the extragalactic distance scale. In particular, the local value of the Hubble constant (H_0) strongly depends on Cepheid distance measurements. The recent *Gaia* Data Releases and other parallax measurements from the *Hubble* Space Telescope (HST) already enabled to improve the accuracy of the slope (α) and intercept (β) of the PL relation. However, the dependence of this law on metallicity is still largely debated. In this paper, we combine three samples of Cepheids in the Milky Way (MW), the Large Magellanic Cloud (LMC) and the Small Magellanic Cloud (SMC) in order to derive the metallicity term (hereafter γ) of the PL relation. The recent publication of extremely precise LMC and SMC distances based on late-type detached eclipsing binary systems (DEBs) provides a solid anchor for the Magellanic Clouds. In the MW, we adopt Cepheid parallaxes from the early third *Gaia* Data Release. We derive the metallicity effect in V , I , J , H , K_S , W_{VI} and W_{JK} . In the K_S band we report a metallicity effect of -0.221 ± 0.051 mag/dex, the negative sign meaning that more metal-rich Cepheids are intrinsically brighter than their more metal-poor counterparts of the same pulsation period.

Keywords: parallaxes – stars: distances – stars: variables: Cepheids – distance scale – metallicity

1. INTRODUCTION

The Cepheid Period-Luminosity (PL) relation, discovered by Henrietta Leavitt (Leavitt & Pickering 1912) about a century ago, is an essential tool for measuring astronomical distances since it represents the first rung of the extragalactic distance ladder. This law is used to measure distances to type Ia supernovae (SNe Ia) host galaxies, and thus plays a key role in the determination of the Hubble constant (H_0). This parameter currently exhibits a tension of at least $\sim 4\sigma$ between its measurement in the early Universe by Planck Collaboration et al.

(2020) assuming a Λ -CDM cosmology and the local estimate based on Cepheid distances (Riess et al. 2021). The precise calibration of the PL relation is therefore of paramount importance to reach a 1% determination of the Hubble constant.

While the slope (α) and intercept (β) of the Leavitt law are generally consistent between various studies, the value and even the sign of the metallicity term (γ , defined as $M = \alpha \log P + \beta + \gamma[\text{Fe}/\text{H}]$) are still debated and constitute 0.5% of the error budget of H_0 (Riess et al. 2016). Some empirical studies report a metallicity dependence consistent with $\gamma \sim 0$ mag/dex: Udalski et al. (2001) concludes with a null-effect from the study of a metal-poor galaxy in optical bands, Storm et al. (2011a) finds a null effect in all bands except in

W_{VI} and [Wielgórski et al. \(2017\)](#) derive a gamma value consistent with zero in optical and NIR bands. Still, a large majority of the analysis investigating the metallicity effect derived a negative sign, with values ranging between -0.2 and -0.5 mag/dex ([Freedman & Madore 1990](#); [Macri et al. 2006](#); [Saha et al. 2006](#); [Gieren et al. 2018](#); [Groenewegen 2018](#)). This trend would indicate that metal-rich Cepheids are brighter than metal-poor ones. However, the study by [Romaniello et al. \(2008\)](#) yielded a metallicity effect of the opposite sign, confirming the theoretical predictions ([Caputo et al. 2000](#); [Bono et al. 2008](#); [Fiorentino et al. 2013](#)).

In this paper, we aim at determining the effect of metallicity on the PL relation by combining samples of Cepheids in the Milky Way (MW) and in the Magellanic Clouds (MCs), taking advantage of the large range of metallicity covered by the Cepheids in these 3 galaxies (from $+0.08$ dex to -0.75 dex). Most of the Cepheids located in distant galaxies hosting SNIa have metallicities within this range, therefore our results are directly applicable to extragalactic studies of the distance scale (e.g. [Javanmardi et al. 2021](#)).

Recently, [Pietrzyński et al. \(2019\)](#) and [Graczyk et al. \(2020\)](#) measured the most precise distances to date for the Large Magellanic Cloud (LMC) and Small Magellanic Cloud (SMC) respectively, based on enhanced samples of late-type detached eclipsing binaries (DEBs). These distances allow us to obtain a precise calibration of the PL relation in the LMC and SMC. For Milky Way (MW) Cepheids, we use the early third *Gaia* Data Release (EDR3) which recently provided parallaxes of unprecedented precision for hundreds of galactic Cepheids.

In Sect. 2, we present our samples of Cepheids in the three galaxies and in Sect. 3 we provide the distances we adopted for each sample. Then in Sect. 4 we estimate the metallicity effect by fitting the Period-Luminosity-Metallicity (PLZ) relation in the three galaxies. We discuss the results in Sect. 5.

2. SAMPLES OF CEPHEIDS

2.1. MW Cepheids

We gather a sample of Milky Way Cepheids for which well-covered light curves are available. In the NIR J , H and K bands, we combine the catalogs by [Welch et al. \(1984\)](#), [Laney & Stobie \(1992\)](#), [Barnes et al. \(1997\)](#) and [Monson & Pierce \(2011\)](#). The data from these four studies are found to be in close agreement, with residuals of 0.013, 0.010 and 0.002 mag in J , H and K respectively ([Monson & Pierce 2011](#)). We adopt these values as photometric zero-point uncertainties for the NIR photometry. Additional NIR data were also found in [Feast](#)

[et al. \(2008\)](#), we consider that including this source of data does not impact the homogeneity and the dispersion of the data since it only affects four stars of the sample. In the optical V and I bands, we use the catalog from [Berdnikov \(2008\)](#) that provides photometry in the Johnson-Cousins system for a large number of Cepheids. Since it is a compilation of data from various catalogs by the same author, we adopt a photometric zero-point uncertainty of 0.010 mag.

For each star and in each filter, we phase the data at the date of maximum luminosity and we obtain intensity-averaged mean apparent magnitudes by performing light curve fitting using Fourier series. Depending on the properties of the different light curves (such as the presence of bumps, steep variations, or to prevent the introduction of unphysical oscillations when the data are too dispersed or not dense enough), we adapt the number of Fourier modes, and thus of free parameters, in order to obtain a satisfactory representation of the light curve. A Fourier decomposition of order three is generally sufficient for an usual Cepheid light curve such as δ Cep, and is up to order six for a more complex star such as RS Pup. We derived the statistical uncertainties on the mean magnitudes from the scatter of each light curve. In some few cases, a very large number of data points are available (> 300) and result in unrealistic small errors: in these cases we adopt a minimum error of 0.006 mag.

For long period Cepheids, large phase shifts may degrade the quality of the fit, the photometry being spread over four decades. Therefore, period changes were taken into account for the phasing of long period stars such as SV Vul, GY Sge or RS Pup ([Kervella et al. 2017](#)). We adopted a polynomial model of up to degree five for the pulsation period.

We carefully analyse the light curves: we exclude Cepheids for which less than 8 data-points are available (MW Cepheids have on average 35 data points in NIR and 160 in optical) and Cepheids that have poor quality photometry or insufficient phase coverage. Finally, we convert all the NIR data in the 2MASS system using the transformations from [Monson & Pierce \(2011\)](#). The systematics related to these transformations are negligible. Examples of a well covered light curve and of a poor-quality light curve are provided in Fig. 8 and 9 in Appendix.

We select Cepheids pulsating in the fundamental mode according to the reclassification by [Ripepi et al. \(2019\)](#). For stars that were not available in this catalog, we adopted by order of priority the pulsation modes from [Groenewegen \(2018\)](#), from the Variable Star index (VSX, [Watson et al. 2006](#)) and from [Luck \(2018\)](#).

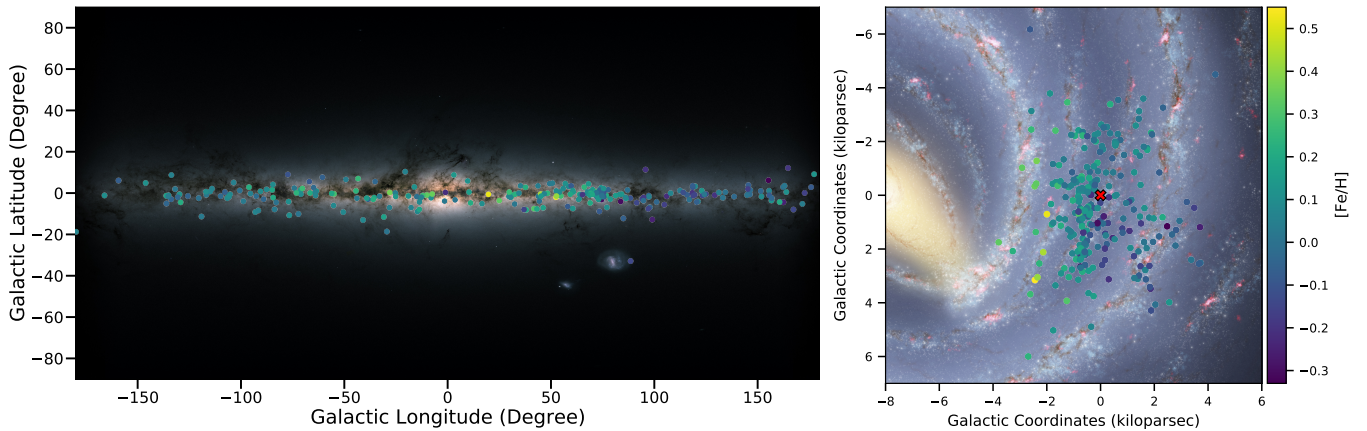


Figure 1. Galactic maps projected on the sky (left) and on the galactic plane (right) showing the distribution of the MW Cepheid sample. The color scale represents the metallicity $[\text{Fe}/\text{H}]$ and the red cross is the position of the Solar System.

We adopt reddening values from Fernie et al. (1995) with a 0.94 scaling factor as suggested by Groenewegen (2018), and from Acharova et al. (2012) if not available in the latter. We adopt an uncertainty of 0.05 if it is not provided.

For MW Cepheids, we search for individual metallicities in Genovali et al. (2015). This catalog provides mean abundances based on high resolution spectra for 75 Cepheids. For stars that are not available in this catalog, we adopt the values from Genovali et al. (2014): they provide homogeneous Cepheid metallicities from their group and compiled from the literature, rescaled to their solar abundance. The individual metallicities are represented in Fig. 1 by colored points, they range from -0.33 dex to $+0.55$ dex. The gradient of metallicity in the MW is particularly visible, with metal-rich Cepheids located closer to the galactic center than metal-poor ones. These individual metallicities have a weighted mean value of 0.083 ± 0.019 dex with a scatter of 0.14 dex. In the following, we adopt this weighted mean value for all MW Cepheids for consistency and homogeneity with the LMC and SMC samples that only have a mean metallicity, but also because the current precision of the individual metallicities is not sufficient for a thorough calibration of the metallicity effect.

The Cepheids of our MW sample are represented in Fig. 1 and their main parameters are listed in Table 4 and Table 5 in Appendix.

2.2. LMC Cepheids

We build a sample of LMC Cepheids by combining the OGLE-IV photometry in V and I bands (Soszyński et al. 2015) with the multi-epoch observations from the LMC Near-Infrared Synoptic Survey by Macri et al. (2015) taken with the CPAPIR camera on the 1.5m CTIO telescope. We update their NIR mean magnitudes to bring

them into better agreement with the 2MASS system using the following relations (L. Macri, priv. comm.). These were derived by matching $\sim 34\,000$ stars in common between their Table A1 and the 2MASS Point Source Catalog (Cutri et al. 2003), with $12 < H < 13.5$, $K > 11.5$ and $-0.5 < J - K < 1.4$ mag:

$$\begin{aligned} J_{2\text{MASS}} &= J_{\text{M15}} - 0.0167 + 0.0205 (J_{\text{M15}} - K_{\text{M15}} - 0.4) \\ &\quad + 0.0101 (J_{\text{M15}} - K_{\text{M15}} - 0.4)^2 \\ H_{2\text{MASS}} &= H_{\text{M15}} + 0.0116 - 0.0054 (J_{\text{M15}} - K_{\text{M15}} - 0.4) \\ &\quad - 0.0189 (J_{\text{M15}} - K_{\text{M15}} - 0.4)^2 \\ K_{2\text{MASS}} &= K_{\text{M15}} + 0.0162 + 0.0227 (J_{\text{M15}} - K_{\text{M15}} - 0.4) \\ &\quad - 0.0595 (J_{\text{M15}} - K_{\text{M15}} - 0.4)^2 \end{aligned}$$

We adopt a photometric zero-point uncertainty of 0.02 mag in all bands. Since some Cepheids exhibit large brightness variations during a pulsation cycle, we consider that single-epoch photometry is not precise enough to derive reliable mean magnitudes, therefore we discarded the mean magnitudes derived by Inno et al. (2016) from template fitting on 2MASS single-point data and IRSF measurements.

We perform a quality check on this initial sample: we reject stars with magnitude uncertainties larger than 1% and with less than 5 data points (LMC Cepheids have on average 43 data points in NIR and 147 in optical), and we only consider fundamental mode Cepheids. We reject Cepheids located outside a radius of 3 degrees around the LMC center in order to avoid outliers such as stars that do not belong to the LMC or that are strongly affected by its geometrical effects (see Sect. 3.2). We adopt reddening values from the Górski et al. (2020) reddening map. The final sample of LMC Cepheids contains 1446 stars in the V band and 807 stars in K_S , it is listed in Table 6 in Appendix and provided as supplementary material online. A map of the final sample of LMC Cepheids is represented in Fig. 2. For

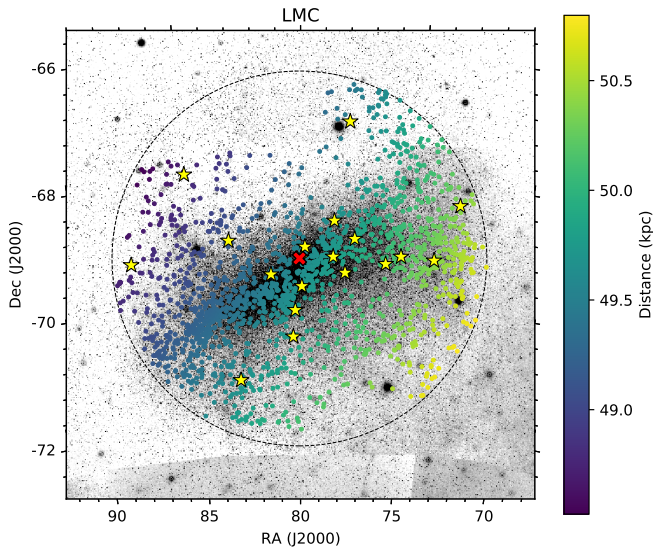


Figure 2. Map of the LMC Cepheids considered in our study. Yellow stars are the eclipsing binaries from Pietrzyński et al. (2019) and the red cross is the center of the LMC. The dashed circle represents a radius of 3 degrees around the LMC center.

LMC Cepheids, we adopt the mean metallicity used by Gieren et al. (2018), that compiles several estimates from various studies: $[Fe/H]_{LMC} = -0.34 \pm 0.06$ dex. The uncertainties take into account the homogenization of the different measurements.

2.3. SMC Cepheids

We assemble a sample of SMC Cepheids by taking the mean magnitudes from the VISTA survey of the Magellanic Clouds (VMC) (Ripepi et al. 2016) cross-matched with OGLE IV photometry by Soszyński et al. (2015). Unfortunately, we do not have H -band photometry for SMC Cepheids because we rejected data from single epoch photometry and template fitting. Results in the H band are therefore derived from the combination of MW and LMC Cepheids only. Magnitudes in the VISTA system were converted into the 2MASS system using the equations from Ripepi et al. (2016):

$$\begin{aligned} J' &= J_{VMC} + 0.070 (J_{VMC} - K_{VMC}) \\ K' &= K_{VMC} - 0.011 (J_{VMC} - K_{VMC}) \end{aligned}$$

We perform an additional correction (L. Macri, priv. comm.) derived by matching ~ 7000 stars in common between the VMC DR4 and the 2MASS Point Source Catalog, with $J > 12.25$, $K > 11.5$ and $-0.5 < J - K < 1.4$ mag:

$$\begin{aligned} J_{2MASS} &= J' - 0.0087 - 0.0010 (J' - K' - 0.4) \\ K_{2MASS} &= K' + 0.0011 - 0.0087 (J' - K' - 0.4) \end{aligned}$$

We adopt a photometric zero-point uncertainty of 0.02 mag for all bands. As we did for the LMC sample, we also reject SMC Cepheids with magnitude uncertainties larger than 1%, with less than 5 data points (SMC Cepheids have on average 17 data points in NIR and 46 in optical) and we only keep Cepheids pulsating in the fundamental mode. As for the LMC sample, we adopt reddening values from the Górski et al. (2020) reddening map.

While the LMC has a rather simple geometry, the SMC is very elongated along the line of sight: we select Cepheids located in a region of 0.6 deg around the SMC center, which covers an area of 1.3 kpc width. Since the SMC distance is derived from detached eclipsing binaries (DEBs), this selection ensures that the Cepheids are located in the same region as these DEBs. The final SMC sample has 284 stars in the V band and 295 stars in K_S , it is listed in Table 7 in Appendix and provided as supplementary material. A map of our final sample of SMC Cepheids is represented in Fig. 3.

For SMC Cepheids, we adopt the mean metallicity used by Gieren et al. (2018), that compiles several estimates from various studies: $[Fe/H]_{SMC} = -0.75 \pm 0.05$ dex. Similar to the LMC value, the uncertainty takes into account the homogenization of the different measurements.

3. DISTANCES

In order to calibrate the Leavitt law, one needs to derive the absolute magnitude of each Cepheid from its apparent luminosity and from its distance.

3.1. Distances to Milky Way Cepheids

Recently, the early third *Gaia* Data Release provided new parallaxes for Milky Way Cepheids (Gaia Collaboration 2020). We perform a first quality check of *Gaia* EDR3 parallaxes based on the Renormalised Unit Weight Error (RUWE) provided in the catalog. This parameter reflects the quality of the parallax of a star compared to other stars of the same color and brightness. Its value is expected to be close to 1 for well-behaved sources (Lindgren et al. 2020a). In particular, the RUWE is sensitive to the photocentric motion of unresolved objects, therefore it can be used to detect possible astrometric binaries. We discard the Cepheids of our sample that have a $RUWE > 1.4$: this selection corresponds to approximately 13 % of our MW sample and removes the stars that are possibly affected by saturation or contamination by a bright neighbour companion. In particular, all the outliers noticed by eye on

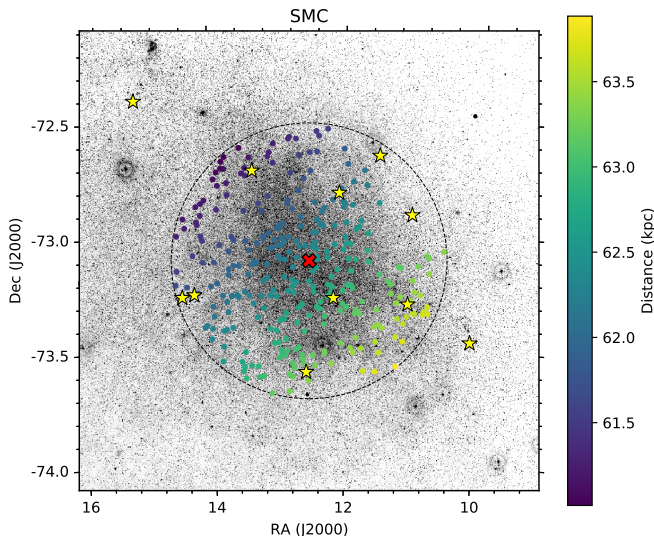


Figure 3. Map of the SMC Cepheids considered in our study. Yellow stars are the eclipsing binaries from Graczyk et al. (2020) and the red cross is the center of the SMC. The dashed circle represents a radius of 0.6 degree around the SMC center.

the PL relation are affected by a large RUWE, therefore the quality check based on this parameter appears to be relevant for our purpose.

Riess et al. (2021) use a different indicator: they identify stars with a goodness of fit (GOF) larger than 12.5 as having a compromised parallax. We find the GOF and the RUWE selections to have a very similar effect on our sample: adopting this GOF criteria for the quality check instead of the RUWE leads to rejecting exactly the same stars, except T Mon, V0496 Aql and VW Pup, that have a RUWE of 1.72, 1.56 and 1.41, and a GOF of 12.11, 10.90 and 11.36 respectively. The RUWE criterion seems slightly more selective than the GOF limit adopted by Riess et al. (2021). Adopting a threshold of $\text{RUWE} < 1.4$ corresponds to a limit GOF of 10.

One method to check if a Cepheid is an astrometric binary is to look for proper motion anomalies between the observations by *Hipparcos* and *Gaia*. Using the approach described in Kervella et al. (2019), we find 20 Cepheids with a high proper motion anomaly signal. However, none of them were identified by their high RUWE or GOF and they do not appear as outliers, therefore we do not exclude them.

Cepheids are variable stars and therefore their brightness and colour can change significantly during a pulsation cycle. This effect was not taken into account in the processing of *Gaia* DR2 astrometry and resulted in additional systematics, noise and dispersion for variable stars parallaxes (Breuval et al. 2020). The correction for this chromatic effect on Cepheid parallaxes is still absent

from *Gaia* EDR3 (Lindgren et al. 2020a). However, the number of observations obtained for each star increased consequently between *Gaia* DR2 (~ 22 months) and *Gaia* EDR3 (~ 34 months). We assume in this paper that the noise induced by this effect is negligible for *Gaia* EDR3 parallaxes.

For each Cepheid we correct for the parallax zero-point (ZP) by using the Python tool¹ described in Lindgren et al. (2020a). This ZP correction takes into account the ecliptic latitude, magnitude and colour of each star. Our MW Cepheids cover a range of magnitudes from $G = 3$ to $G = 12$ mag. For our sample of MW Cepheids, we find the ZP to vary between -4 and $-54 \mu\text{as}$ with a median value of $-27 \mu\text{as}$ ($\sigma = 10 \mu\text{as}$), which is very similar to the median parallax offset derived by Riess et al. (2021). Following Lindgren et al. (2020a) who recommend to include an uncertainty of a few micro arcseconds in the ZP, we adopt a systematic error of $5 \mu\text{as}$ on this quantity. Considering our sample of Cepheids, this error is equivalent to an average systematic uncertainty of 0.020 mag in distance modulus. In Sect. 5.1, we discuss the influence of adopting this individual ZP correction compared with the uniform ZP of $-17 \mu\text{as}$ derived from quasars.

We find 13 Cepheids to fall in the range between $G = 10.8$ and $G = 11.2$ mag, where a transition of window classes occurs (Fig. 1 in Lindgren et al. 2020b). In this particular range, the value of the parallax zero-point can possibly be affected so we quadratically add $10 \mu\text{as}$ to the parallax uncertainty.

Finally, we increase all *Gaia* EDR3 parallax uncertainties by 10%, following Riess et al. (2021) to account for potential excess uncertainty. This correction has significantly reduced since *Gaia* DR2, where it was recommended to increase parallax uncertainties by 30%.

3.2. Distances to LMC Cepheids

Recently, Pietrzyński et al. (2019) estimated the distance to the LMC with a 1% precision based on detached-eclipsing binaries (DEBs): $d_{\text{LMC}} = 49.59 \pm 0.09$ (stat.) ± 0.54 (syst.) kpc. This method for measuring distances is independent from Cepheids and relies on surface-brightness relations, established by precise interferometric measurements. We use this value as initial distance to our Cepheids and we add a corrective term depending on the position of each Cepheid in the LMC, assuming the disc geometry derived by OGLE from Cepheids by Jacyszyn-Dobrzniecka et al. (2016). First

¹ <https://www.cosmos.esa.int/web/gaia/edr3-code>

we compute the cartesian coordinates (x_i, y_i, z_i) of each Cepheid from their equatorial coordinates (α_i, δ_i) using the transformations:

$$\begin{cases} x_i = -d_{\text{LMC}} \cos \delta_i \sin(\alpha_i - \alpha_{\text{LMC}}) \\ y_i = d_{\text{LMC}} [\sin \delta_i \cos \delta_{\text{LMC}} \\ \quad - \cos \delta_i \sin \delta_{\text{LMC}} \cos(\alpha_i - \alpha_{\text{LMC}})] \\ z_i = c_1 x_i + c_2 y_i + d_{\text{LMC}} \end{cases}$$

where $(\alpha_{\text{LMC}}, \delta_{\text{LMC}}) = (80.05, -69.30)$ deg are the coordinates of the LMC center and the coefficients $(c_1, c_2) = (0.395 \pm 0.014, -0.215 \pm 0.013)$ are from [Jacyszyn-Dobrzniecka et al. \(2016\)](#). The corrected distance of each LMC Cepheid is:

$$d_i = \sqrt{x_i^2 + y_i^2 + z_i^2}$$

The distances of each LMC Cepheid derived with this correction are located in a range of ± 1.5 kpc around the mean LMC distance from [Pietrzyński et al. \(2019\)](#). They are represented by the colors in Fig. 2.

3.3. Distances to SMC Cepheids

The distance to the SMC was recently measured by [Graczyk et al. \(2020\)](#) with a precision of 1.5 % using the same method as used in [Pietrzyński et al. \(2019\)](#) for the LMC: from a sample of 15 DEBs, a distance of $d_{\text{SMC}} = 62.44 \pm 0.47$ (stat.) ± 0.81 (syst.) kpc is derived. However, the SMC has a large extension along the line of sight ([Subramanian & Subramaniam 2012](#); [Jacyszyn-Dobrzniecka et al. 2016](#); [Ripepi et al. 2017](#)), which makes the distance to its core region particularly difficult to measure, contrary to the LMC that has a rather simple geometry. In this section, we take into account the SMC elongated shape in order to derive corrected distances to each of its Cepheids. For each SMC Cepheid of coordinates (α_i, δ_i) , we compute the cartesian coordinates (x_i, y_i) such that:

$$\begin{cases} x_i = -d_{\text{SMC}} \cos \delta_i \sin(\alpha_i - \alpha_{\text{SMC}}) \\ y_i = d_{\text{SMC}} [\sin \delta_i \cos \delta_{\text{SMC}} \\ \quad - \cos \delta_i \sin \delta_{\text{SMC}} \cos(\alpha_i - \alpha_{\text{SMC}})] \end{cases}$$

where $(\alpha_{\text{SMC}}, \delta_{\text{SMC}}) = (12.54, -73.11)$ deg ([Ripepi et al. 2017](#)). Then we used the equations corresponding to the blue lines in Fig. 4 of [Graczyk et al. \(2020\)](#):

$$\begin{cases} d_i(x) = (3.086 \pm 0.066) x_i + d_{\text{SMC}} \\ d_i(y) = (-3.248 \pm 0.118) y_i + d_{\text{SMC}} \end{cases}$$

We adopt the mean value of $d_i(x)$ and $d_i(y)$ as the final distance of each Cepheid. The elongated shape of

Table 1. Results of the PL fit of the form $M = \alpha(\log P - 0.7) + \beta$ in the Milky Way, the Large Magellanic Cloud and the Small Magellanic Cloud.

Band	α	β	σ	$N^{(*)}$
MW ^(a)				
<i>V</i>	-2.443 ± 0.031	-3.296 ± 0.024	0.25	178
<i>I</i>	-2.780 ± 0.028	-3.981 ± 0.024	0.23	150
<i>W_{VI}</i>	-3.289 ± 0.026	-5.030 ± 0.025	0.21	149
<i>J</i>	-3.050 ± 0.029	-4.498 ± 0.026	0.18	97
<i>H</i>	-3.160 ± 0.028	-4.762 ± 0.024	0.17	97
<i>K_S</i>	-3.207 ± 0.028	-4.848 ± 0.022	0.17	97
<i>W_{JK}</i>	-3.317 ± 0.028	-5.086 ± 0.026	0.17	97
LMC ^(b)				
<i>V</i>	-2.704 ± 0.007	-3.284 ± 0.033	0.23	1446
<i>I</i>	-2.916 ± 0.005	-3.910 ± 0.033	0.15	1460
<i>W_{VI}</i>	-3.281 ± 0.008	-4.877 ± 0.038	0.08	1432
<i>J</i>	-3.127 ± 0.005	-4.385 ± 0.033	0.12	805
<i>H</i>	-3.160 ± 0.005	-4.696 ± 0.033	0.11	808
<i>K_S</i>	-3.217 ± 0.005	-4.737 ± 0.033	0.10	807
<i>W_{JK}</i>	-3.272 ± 0.008	-4.974 ± 0.039	0.10	806
SMC ^(c)				
<i>V</i>	-2.594 ± 0.012	-3.196 ± 0.038	0.28	284
<i>I</i>	-2.871 ± 0.008	-3.841 ± 0.038	0.22	297
<i>W_{VI}</i>	-3.334 ± 0.014	-4.834 ± 0.043	0.12	283
<i>J</i>	-2.956 ± 0.004	-4.317 ± 0.038	0.17	294
<i>H</i>	—	—	—	—
<i>K_S</i>	-3.163 ± 0.002	-4.670 ± 0.038	0.15	295
<i>W_{JK}</i>	-3.326 ± 0.002	-4.916 ± 0.043	0.14	295

NOTE—(*) The number of stars is given after the sigma clipping procedure and the period cuts.

(a) Mean $[\text{Fe}/\text{H}] = +0.083 \pm 0.019$ dex

(b) Mean $[\text{Fe}/\text{H}] = -0.34 \pm 0.06$ dex

(c) Mean $[\text{Fe}/\text{H}] = -0.75 \pm 0.05$ dex

the SMC is highlighted by the dispersion of the derived distances between +5 kpc and -6 kpc around the mean value d_{SMC} , which represents almost 10% of the mean value. The distances of our sample of SMC Cepheids are represented on the map in Fig. 3. A discussion about the elongated shape of the SMC and its impact on our results is provided in Sect. 5.2.

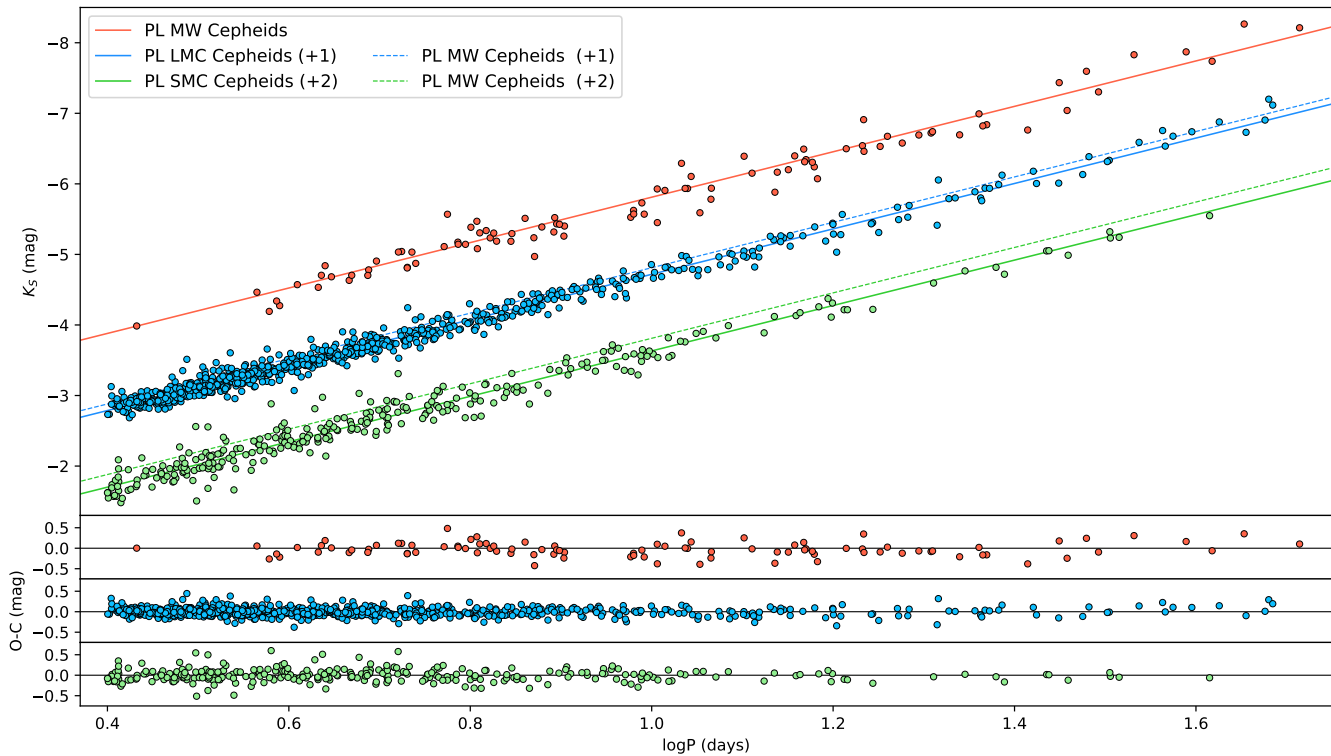


Figure 4. Fit of the PL relation in K_S for MW, LMC and SMC Cepheids. The lower panel shows the residual between the Cepheid absolute magnitudes and the corresponding PL fit for each of the three galaxies. The LMC and SMC relations were offset by +1 and +2 mag, respectively, for visualization purposes.

4. THE METALLICITY EFFECT FROM MILKY WAY AND MAGELLANIC CLOUD CEPHEIDS

In this section, we aim at estimating the metallicity term γ of the Leavitt law. In Sect. 4.1, we start by fitting the α and β coefficients of the PL relation in each of the three galaxies, without considering the metallicity term. In Sect. 4.2, we include the metallicity for each galaxy and derive the third term of the PLZ relation by combining the three galaxies.

4.1. The Period-Luminosity relation

We adopt the Cepheid samples described in Sect. 2. In a first place, we correct apparent magnitudes for the extinction by adopting the reddening law from Cardelli et al. (1989) and O’Donnell (1994) assuming $R_V = 3.135$ which yields $A_\lambda = R_\lambda E(B - V)$ with $R_I = 1.894$, $R_J = 0.892$, $R_H = 0.553$ and $R_{K_S} = 0.363$. We also derive optical and NIR Wesenheit indices (Madore 1982) as defined by $W_{VI} = I - 1.526 (V - I)$ and $W_{JK} = K_S - 0.686 (J - K_S)$. Wesenheit magnitudes are particularly convenient for calibrating the PL relation since they are independent of reddening.

We account for the width of the instability strip by adding quadratically to the photometry uncertainties

the intrinsic scatter in each band: this quantity is obtained by subtracting quadratically the measurement errors (photometric inhomogeneities, differential extinction, geometrical effects, phase corrections, etc) from the scatter of the PL relation: we adopt a width of the instability strip of 0.07 mag in NIR bands (J , H , K_S and W_{JK}) from Persson et al. (2004), 0.15 mag in V and 0.09 mag in I from Macri et al. (2006) and finally 0.08 mag in W_{VI} from Madore et al. (2017). We derive the absolute magnitude M_λ of each Cepheid from their distance d (in kpc) and dereddened apparent magnitude m_λ :

$$M_\lambda = m_\lambda - 5 \log d - 10 \quad (1)$$

In the Milky Way, the distance is obtained at the first order by taking the inverse of the parallax. In order to avoid biases due to this inversion, we adopt the approach introduced by Feast & Catchpole (1997) and Arenou & Luri (1999), consisting in fitting the Astrometric Based Luminosity (ABL) function instead of absolute magnitudes:

$$\text{ABL} = \pi_{(\text{mas})} 10^{0.2m_\lambda - 2} = 10^{M_\lambda/5} \quad (2)$$

where:

$$M_\lambda = \alpha_\lambda (\log P - \log P_0) + \beta_\lambda \quad (3)$$

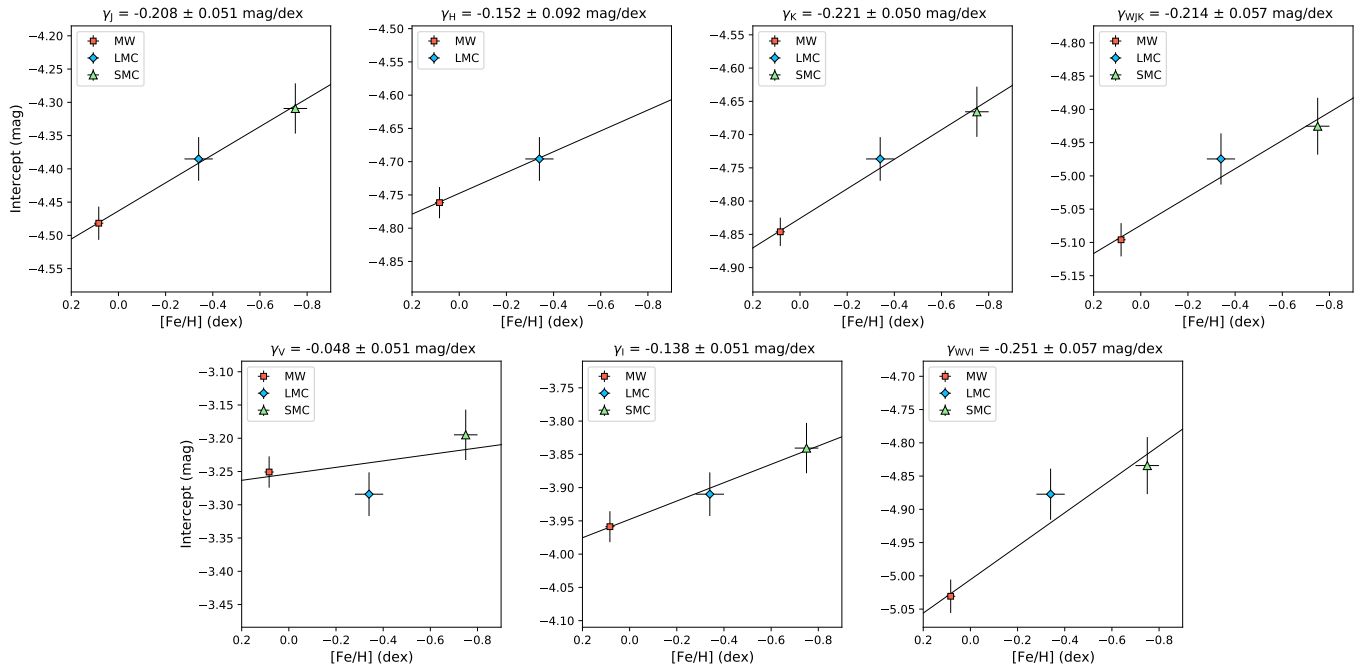


Figure 5. Intercept of the PL relation represented as a function of metallicity in J , H , K , V , I , and Wesenheit bands.

We adopt a pivot period of $\log P_0 = 0.7$ which represents the median period of our Cepheid sample. This approach ensures minimum correlations between the fitted coefficients. We perform a 3σ clipping procedure on the PL relation to remove possible outliers.

A non-linearity in the SMC PL relation was highlighted at the short-periods end ($\log P < 0.4$) (EROS Collaboration et al. 1999). For LMC and SMC Cepheids, Chown et al. (2021) detect a break in the PL relation at $\log P = 0.29$ and also at very long periods ($\log P = 1.72$). Cepheids beyond these limits are found to deviate from the global PL fit and can affect both the slope and the zero-point. Additionally, the short-period edge of the PL relation is potentially affected by first-overtone contamination. In the following, we exclude all Cepheids with periods shorter than 2.5 days ($\log P = 0.4$) and longer than 52 days ($\log P = 1.72$). Finally, we include the systematics on the LMC and SMC distance moduli (respectively 0.026 mag and 0.032 mag) and the photometric zero-points provided in Sect. 2 on the intercept error. We use the `curve_fit` function from the `scipy` Python library in a Monte Carlo algorithm to derive the PL coefficients and the 16th and 84th percentiles of the distribution to derive the uncertainties. The PL relations derived for each galaxy are provided in Table 1, where both the slope and intercept are fitted.

In each band, the intercept increases with decreasing metallicity, i.e. it becomes less negative from the MW to the LMC and in turn to the SMC. In the NIR, the

intercept changes by ~ 0.18 mag between the MW and the SMC, possibly indicating a strong dependence with metallicity. We note that our K_S band calibration in the MW is in good agreement with the result by Breuval et al. (2020) based on *Gaia* DR2 parallaxes. The fit of the PL relation in the K_S band performed in each of the three galaxies is represented in Fig. 4.

4.2. The Period-Luminosity-Metallicity relation

In this section, we now calibrate the dependence of the PL intercept β with metallicity. First, we fit the PL relation of the form $M = \alpha(\log P - 0.7) + \beta$ in each of the three galaxies separately with a common slope fixed to the LMC value. As in previous section, the systematics due to the LMC and SMC distance and to the photometric zero-point are included in quadrature to the intercept random error. The intercept β contains the metallicity term such that:

$$\beta = \gamma [\text{Fe}/\text{H}] + \delta \quad (4)$$

In Fig. 5 are represented the intercepts of the PL relations in the MW, LMC and SMC as a function of metallicity. We fit Eq. 4 with a Monte Carlo algorithm to derive the γ and δ coefficients, and we adopt the 16th and 84th percentiles of the distribution to derive the random errors. A histogram representing the distribution of the γ values obtained with the Monte Carlo algorithm is represented in Fig. 6.

The results of the fit are listed in Table 2. In the NIR, we report a strong metallicity effect of $-0.208 \pm$

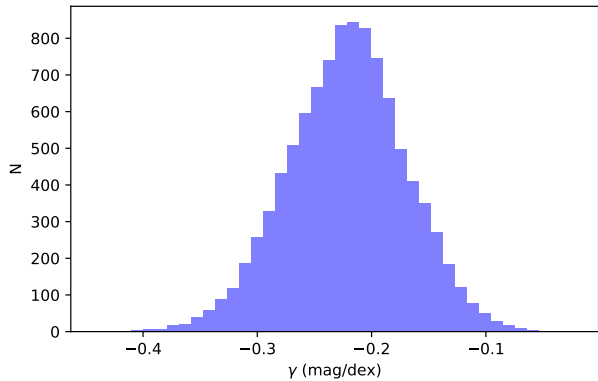


Figure 6. Histogram of the γ values obtained in the K_S band by the Monte Carlo algorithm iterated 10 000 times.

0.051 mag/dex in J , -0.152 ± 0.092 mag/dex in H and -0.221 ± 0.050 mag/dex in K_S . The NIR Wesenheit index W_{JK} shows a similar dependence with -0.214 ± 0.057 mag/dex. These results agree by 1σ with Gieren et al. (2018), who used the Infrared Surface Brightness Technique (Fouqué & Gieren 1997; Storm et al. 2011b) to derive the distances to the Cepheids in their MW, LMC and SMC samples, an approach different and independent from the one used in the present study. In the NIR Wesenheit index W_H , Riess et al. (2019) find an effect of -0.170 ± 0.060 mag/dex, which is also close to our results in the NIR. In optical bands, we derive a weaker effect than in the NIR with -0.048 ± 0.051 mag/dex in V and of -0.138 ± 0.051 mag/dex in I . These values also agree at 1σ with Gieren et al. (2018), and the value in V is also consistent at 1σ with the differential study of LMC and SMC PL relations by Wielgórski et al. (2017). On average, our results are located between the values by Wielgórski et al. (2017), consistent with a null metallicity effect, and the work by Gieren et al. (2018) that derive a strong negative effect. In the H band, we derive a metallicity effect weaker than in other NIR bands, likely because it is derived from the MW and LMC samples only (due to the lack of H -band photometry for SMC Cepheids). We conclude with the general trend being that the sensitivity to metallicity increases in absolute sense and becomes more negative from optical to NIR wavelengths. This trend is particularly visible in Fig. 7.

We note that the PL slope was fixed to the LMC value because this sample contains significantly more stars than the two other ones. However, if the slope is fixed to the value found in the Milky Way or in the SMC, the intercepts agree by 0.2% in NIR and by 1.4% in optical. Similarly, the γ values agree at 0.2σ and 0.8

Table 2. Final results of the PLZ fit of the form $M = \alpha(\log P - 0.7) + \delta + \gamma [\text{Fe}/\text{H}]$ and associated uncertainties.

Band	α	σ	δ	σ	γ	σ
V	-2.704	0.007	-3.252	0.020	-0.048	0.055
I	-2.916	0.005	-3.948	0.020	-0.138	0.053
W_{VI}	-3.281	0.008	-5.005	0.022	-0.251	0.057
J	-3.127	0.005	-4.463	0.022	-0.208	0.052
H	-3.160	0.005	-4.748	0.020	-0.152	0.092
K_S	-3.217	0.004	-4.826	0.019	-0.221	0.051
W_{JK}	-3.273	0.008	-5.075	0.022	-0.214	0.057

NOTE—The uncertainties include the systematics discussed in Sect. 5.2.

σ in NIR and optical respectively.

5. DISCUSSION

The metallicity term of the PL relation can be sensitive to many different effects. In this section we study the stability γ after varying some parameters.

5.1. Influence of Gaia EDR3 parallax zero-point

In Sect. 3.1, we corrected each *Gaia* EDR3 parallax for their individual zero-point by using the Python tool described in Lindegren et al. (2020a). However, in Lindegren et al. (2020b), a uniform parallax zero-point of $-17\mu\text{as}$ is derived from quasars. The results of the PLZ fit obtained after adopting this uniform zero-point are provided in the second part of Table 3 in appendix. They are consistent at the 1σ level with the values derived using the individual zero-point, although it gives a slightly more negative metallicity effect in each band. For example, in K_S we obtain $\gamma = -0.271 \pm 0.051$ mag/dex compared with $\gamma = -0.221 \pm 0.050$ mag/dex with individual zero-points. This effect can be explained by the individual zero-points being on average more negative than $-17\mu\text{as}$ for our sample of MW Cepheids.

We also investigate whether the individual zero-point correction by Lindegren et al. (2020a) is adapted to the most distant Cepheids: we remove from our sample the Cepheids with a parallax smaller than 0.3mas and derive the PL relation in K_S without these stars. Using this PL relation, we compute the expected parallax of the most distant Cepheids and compare it with the *Gaia* EDR3 parallax corrected by the individual zero-point. We find a good agreement between the predicted parallaxes and the values from *Gaia* EDR3 with the Lindegren et al. (2020a) individual correction. From this study, we confirm that the individual zero-point

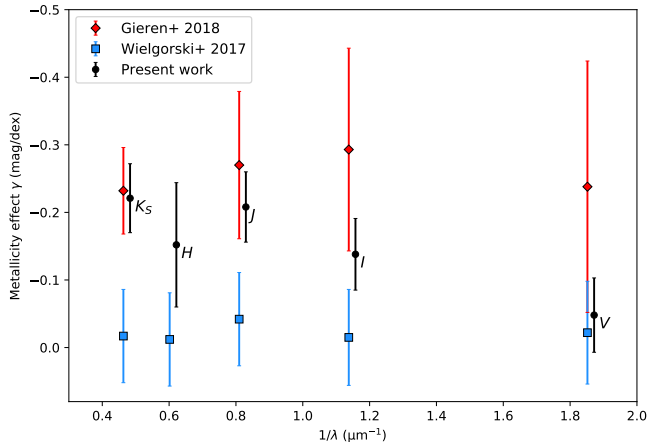


Figure 7. Metallicity effect as a function of wavelength, compared with values from the literature. The error bars include the systematics discussed in Sect. 5.2. For visualization purposes, the X axis was slightly shifted for our values so that the error bars do not overlap, but they correspond to the same wavelength as the literature values.

correction from Lindegren et al. (2020a) is adapted to the most distant MW Cepheids of our sample.

5.2. Influence of the SMC sample

As mentioned in Sect. 2.3 and 3.3, the distance to the core region of the SMC is particularly difficult to measure. From their sample of DEBs, Graczyk et al. (2020) derive an uncertainty of about 2% for the distance to the SMC core region. These DEB systems are unevenly distributed in the central region of the galaxy and their individual distances show a large dispersion around the mean value, ranging from 57 kpc to 67 kpc (see their Fig. 3), which corresponds to $\sim 16\%$ of the SMC distance. In order to avoid including Cepheids located too far away from the SMC center, we restricted our sample to a region of radius 0.6 degree around the SMC center. With a smaller radius, the contribution of the SMC sample in the PLZ fit becomes smaller than the MW contribution, therefore we consider that the number of retained SMC Cepheids is insufficient. On the other hand, if we assume a radius larger than 0.6 deg around the SMC center, the number of outlier stars increases and the distance of some Cepheids may not correspond to the distance of the SMC core region. In order to test the validity of our hypothesis, we perform the same PLZ fit with a radius of 0.5 and 0.7 deg around the SMC center and report the coefficients in Table 3.

After extending the SMC sample to a radius of 0.7 degree around the galaxy center, we find γ values in very good agreement (better than 1σ) with the values derived in the initial conditions. When the radius is

reduced to 0.5 degree, the metallicity effect still agrees at 1σ with the initial conditions in all bands. Considering a smaller region around the SMC center results in a slightly stronger (i.e. more negative) metallicity effect. These results highlight the sensitivity of the metallicity effect with respect to the adopted SMC sample, and in particular to the spatial distribution of the Cepheids considered. Moreover, it emphasizes the necessity to correct each Cepheid distance according to their position in the SMC plane, as we did in Sect. 3.3.

We consider the variation of γ within a region of $0.5^\circ < R < 0.7^\circ$ around the SMC center as an additional source of systematic uncertainties: this source of error is at the level of 0.02 mag/dex in optical bands and of 0.01 mag/dex in NIR (see Table 3). We adopt the same additional source of uncertainty for the intercept δ , although the latter coefficient is particularly stable when the radius around the SMC center is changed. These systematics are included in the results presented in Table 2.

6. CONCLUSIONS

We build large samples of Cepheids in the Milky Way and in the Magellanic Clouds and make use of the most recent and precise distances available to estimate the metallicity effect on the Cepheid PL relation. In the K_S band we derive an effect of $\gamma = -0.221 \pm 0.051$ mag/dex, in agreement with the value found by Gieren et al. (2018) but more precise. In the V band we derive a weaker effect of $\gamma = -0.048 \pm 0.055$ mag/dex, which is consistent with both Wielgórski et al. (2017) and Gieren et al. (2018) within the error bars. We conclude with a non-zero dependence of Cepheid magnitude with metallicity and we confirm its negative sign: metal-rich Cepheids are brighter than metal-poor ones.

The improved precision reached in this work was made possible thanks to the high quality of *Gaia* EDR3 parallaxes and to the new distances of the two Magellanic Clouds obtained by the Araucaria Project. Combining Milky Way and Magellanic Cloud Cepheids also allows to reach a better precision than previous studies based on Magellanic Clouds only, by the larger range of metallicities they cover. A refined analysis of each light curve ensures the use of accurate mean magnitudes. However, the elongated shape of the SMC in the line of sight remains a source of systematic uncertainty in our study, despite continuous efforts to improve our knowledge of its structure. In this study, we assumed a linear dependence of the PL relation with metallicity, but it might as well be non-linear (Gieren et al. 2018). Additional high resolution spectroscopic metallicity mea-

surements of both Milky Way and Magellanic Cloud Cepheids should be carried out in the future to even better constrain the metallicity effect, particularly in the NIR, in our effort to further reduce the systematic uncertainty on the determination of the Hubble constant from the Cepheid-SN Ia method.

ACKNOWLEDGMENTS

We thank the anonymous referee for the very constructive comments that helped us to improve the manuscript. We are grateful to Lucas Macri for providing the photometric transformations. The research leading to these results has received funding from the European Research Council (ERC) under the European Union’s Horizon 2020 research and innovation programme under grant agreement No 695099 (project CepBin). This work has made use of data from the European Space Agency (ESA) mission Gaia (<http://www.cosmos.esa.int/gaia>), processed by the Gaia Data Processing and Analysis Consortium (DPAC, <http://www.cosmos.esa.int/web/gaia/dpac/consortium>). Funding for the DPAC has been provided by national institutions, in particular the institutions participating in the Gaia Multilateral Agreement. The authors acknowledge the support of the French Agence Nationale de la Recherche (ANR), under grant ANR-15-CE31-0012-01 (project UnlockCepheids). W.G. and G. P. gratefully acknowledge financial support for this work from the BASAL Centro de Astrofísica y Tecnologías Afines (CATA) AFB- 170002. W.G. and D. G. acknowledge financial support from the Millenium Institute of Astrophysics (MAS) of the Iniciativa Científica Milenio del Ministerio de Economía, Fomento y Turismo de Chile, project IC120009. This research made use of Astropy7, a community-developed core Python package for Astronomy ([Astropy Collaboration et al. 2018](#)). Support from the Polish National Science Centre grants MAESTRO UMO-2017/26/A/ST9/00446 and from the IdPPII 2015 0002 64 and DIR/WK/2018/12 grants of the Polish Ministry of Science and Higher Education is also acknowledged. We used the SIMBAD and VIZIER databases and catalog access tool at the CDS, Strasbourg (France), and NASA’s Astrophysics Data System Bibliographic Services.

REFERENCES

- Acharova, I. A., Mishurov, Y. N., & Kovtyukh, V. V. 2012, *MNRAS*, 420, 1590
- Arenou, F., & Luri, X. 1999, in *Astronomical Society of the Pacific Conference Series*, Vol. 167, *Harmonizing Cosmic Distance Scales in a Post-HIPPARCOS Era*, ed. D. Egret & A. Heck, 13–32
- Astropy Collaboration, Price-Whelan, A. M., Sipőcz, B. M., et al. 2018, *AJ*, 156, 123
- Barnes, T. G., I., Fernley, J. A., Frueh, M. L., et al. 1997, *Publications of the Astronomical Society of the Pacific*, 109, 645
- Berdnikov, L. N. 2008, *VizieR Online Data Catalog*, 2285, 0
- Bono, G., Caputo, F., Fiorentino, G., Marconi, M., & Musella, I. 2008, *ApJ*, 684, 102
- Breuval, L., Kervella, P., Anderson, R. I., et al. 2020, *A&A*, 643, A115
- Caputo, F., Marconi, M., Musella, I., & Santolamazza, P. 2000, *A&A*, 359, 1059
- Cardelli, J. A., Clayton, G. C., & Mathis, J. S. 1989, *ApJ*, 345, 245
- Chown, A. H., Scowcroft, V., & Wuyts, S. 2021, *MNRAS*, 500, 817
- Cutri, R. M., Skrutskie, M. F., van Dyk, S., et al. 2003, *2MASS All Sky Catalog of point sources*.
- EROS Collaboration, Bauer, F., Afonso, C., et al. 1999, *A&A*, 348, 175
- Feast, M. W., & Catchpole, R. M. 1997, *MNRAS*, 286, L1, doi: [10.1093/mnras/286.1.L1](https://doi.org/10.1093/mnras/286.1.L1)
- Feast, M. W., Laney, C. D., Kinman, T. D., van Leeuwen, F., & Whitelock, P. A. 2008, *MNRAS*, 386, 2115, doi: [10.1111/j.1365-2966.2008.13181.x](https://doi.org/10.1111/j.1365-2966.2008.13181.x)
- Fernie, J. D., Evans, N. R., Beattie, B., & Seager, S. 1995, *Information Bulletin on Variable Stars*, 4148
- Fiorentino, G., Musella, I., & Marconi, M. 2013, *MNRAS*, 434, 2866
- Fouqué, P., & Gieren, W. P. 1997, *A&A*, 320, 799
- Freedman, W. L., & Madore, B. F. 1990, *ApJ*, 365, 186
- Gaia Collaboration. 2020, *VizieR Online Data Catalog*, I/350
- Genovali, K., Lemasle, B., Bono, G., et al. 2013, *A&A*, 554, A132
- . 2014, *A&A*, 566, A37, doi: [10.1051/0004-6361/201323198](https://doi.org/10.1051/0004-6361/201323198)
- Genovali, K., Lemasle, B., da Silva, R., et al. 2015, *A&A*, 580, A17
- Gieren, W., Storm, J., Konorski, P., et al. 2018, *A&A*, 620, A99, doi: [10.1051/0004-6361/201833263](https://doi.org/10.1051/0004-6361/201833263)
- Górski, M., Zgirski, B., Pietrzyński, G., et al. 2020, *ApJ*, 889, 179
- Graczyk, D., Pietrzyński, G., Thompson, I. B., et al. 2020, *arXiv e-prints*, arXiv:2010.08754
- Groenewegen, M. A. T. 2018, *A&A*, 619, A8, doi: [10.1051/0004-6361/201833478](https://doi.org/10.1051/0004-6361/201833478)
- Inno, L., Bono, G., Matsunaga, N., et al. 2016, *ApJ*, 832, 176
- Jacyszyn-Dobrzeńska, A. M., Skowron, D. M., Mróz, P., et al. 2016, *AcA*, 66, 149
- Javanmardi, B., Mérand, A., Kervella, P., et al. 2021, *arXiv e-prints*, arXiv:2102.12489
- Kervella, P., Arenou, F., Mignard, F., & Thévenin, F. 2019, *A&A*, 623, A72, doi: [10.1051/0004-6361/201834371](https://doi.org/10.1051/0004-6361/201834371)
- Kervella, P., Trahin, B., Bond, H. E., et al. 2017, *A&A*, 600, A127, doi: [10.1051/0004-6361/201630202](https://doi.org/10.1051/0004-6361/201630202)
- Laney, C. D., & Stobie, R. S. 1992, *A&AS*, 93, 93
- Leavitt, H. S., & Pickering, E. C. 1912, *Harvard College Observatory Circular*, 173, 1
- Lemasle, B., François, P., Bono, G., et al. 2007, *A&A*, 467, 283
- Lindegren, L., Klioner, S. A., Hernández, J., et al. 2020a, *arXiv e-prints*, arXiv:2012.03380
- Lindegren, L., Bastian, U., Biermann, M., et al. 2020b, *arXiv e-prints*, arXiv:2012.01742
- Luck, R. E. 2018, *AJ*, 156, 171, doi: [10.3847/1538-3881/aadcac](https://doi.org/10.3847/1538-3881/aadcac)
- Luck, R. E., Andrievsky, S. M., Kovtyukh, V. V., Gieren, W., & Graczyk, D. 2011, *AJ*, 142, 51
- Luck, R. E., & Lambert, D. L. 2011, *AJ*, 142, 136
- Macri, L. M., Ngeow, C.-C., Kanbur, S. M., Mahzooni, S., & Smitka, M. T. 2015, *AJ*, 149, 117
- Macri, L. M., Stanek, K. Z., Bersier, D., Greenhill, L. J., & Reid, M. J. 2006, *ApJ*, 652, 1133
- Madore, B. F. 1982, *ApJ*, 253, 575
- Madore, B. F., Freedman, W. L., & Moak, S. 2017, *ApJ*, 842, 42
- Monson, A. J., & Pierce, M. J. 2011, *ApJS*, 193, 12, doi: [10.1088/0067-0049/193/1/12](https://doi.org/10.1088/0067-0049/193/1/12)
- O'Donnell, J. E. 1994, *ApJ*, 422, 158
- Pedicelli, S., Lemasle, B., Groenewegen, M., et al. 2010, *A&A*, 518, A11
- Persson, S. E., Madore, B. F., Krzemiński, W., et al. 2004, *AJ*, 128, 2239
- Pietrzyński, G., Graczyk, D., Gallenne, A., et al. 2019, *Nature*, 567, 200
- Planck Collaboration, Aghanim, N., Akrami, Y., et al. 2020, *A&A*, 641, A6, doi: [10.1051/0004-6361/201833910](https://doi.org/10.1051/0004-6361/201833910)
- Riess, A. G., Casertano, S., Yuan, W., et al. 2021, *ApJL*, 908, L6

- Riess, A. G., Casertano, S., Yuan, W., Macri, L. M., & Scolnic, D. 2019, *ApJ*, 876, 85
- Riess, A. G., Macri, L. M., Hoffmann, S. L., et al. 2016, *ApJ*, 826, 56, doi: [10.3847/0004-637X/826/1/56](https://doi.org/10.3847/0004-637X/826/1/56)
- Ripepi, V., Molinaro, R., Musella, I., et al. 2019, *A&A*, 625, A14
- Ripepi, V., Marconi, M., Moretti, M. I., et al. 2016, *ApJS*, 224, 21
- Ripepi, V., Cioni, M.-R. L., Moretti, M. I., et al. 2017, *MNRAS*, 472, 808
- Romaniello, M., Primas, F., Mottini, M., et al. 2008, *A&A*, 488, 731
- Saha, A., Thim, F., Tammann, G. A., Reindl, B., & Sandage, A. 2006, *ApJS*, 165, 108
- Soszyński, I., Udalski, A., Szymański, M. K., et al. 2015, *AcA*, 65, 297. <https://arxiv.org/abs/1601.01318>
- Storm, J., Gieren, W., Fouqué, P., et al. 2011a, *A&A*, 534, A95
- . 2011b, *A&A*, 534, A94
- Subramanian, S., & Subramaniam, A. 2012, *ApJ*, 744, 128
- Sziládi, K., Vinkó, J., Poretti, E., Szabados, L., & Kun, M. 2007, *A&A*, 473, 579
- Udalski, A., Wyrzykowski, L., Pietrzynski, G., et al. 2001, *AcA*, 51, 221
- Watson, C. L., Henden, A. A., & Price, A. 2006, *Society for Astronomical Sciences Annual Symposium*, 25, 47
- Welch, D. L., Wieland, F., McAlary, C. W., et al. 1984, *ApJS*, 54, 547, doi: [10.1086/190943](https://doi.org/10.1086/190943)
- Wielgórski, P., Pietrzyński, G., Gieren, W., et al. 2017, *ApJ*, 842, 116
- Yong, D., Carney, B. W., Teixeira de Almeida, M. L., & Pohl, B. L. 2006, *AJ*, 131, 2256

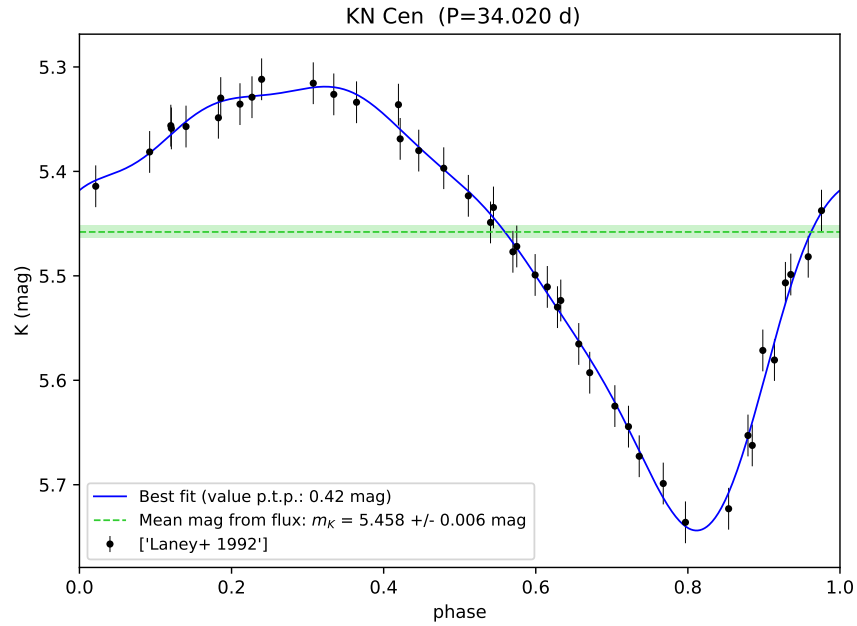


Figure 8. Example of a well covered light curve in the K band for the Galactic Cepheid KN Cen. The solid blue line represents the best fit of the light curve, the dashed green line is the mean magnitude derived from the best fit and the green region is the uncertainty on the intensity-averaged mean magnitude.

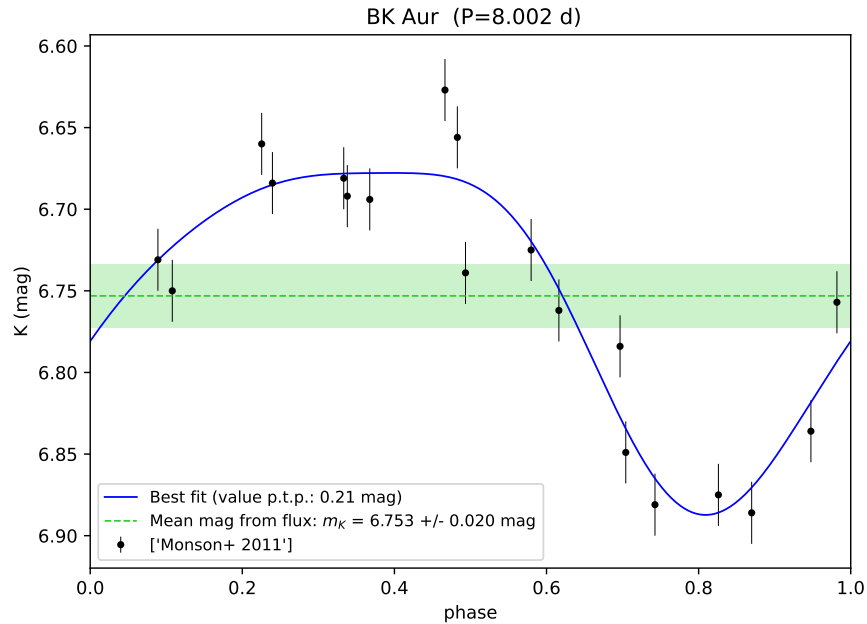


Figure 9. Example of a poor-quality light curve in the K band for the Galactic Cepheid BK Aur. The solid blue line represents the best fit of the light curve, the dashed green line is the mean magnitude derived from the best fit and the green region is the uncertainty on the intensity-averaged mean magnitude.

Table 3. Results of the PLZ linear fit of the form $M = \alpha(\log P - 0.7) + \delta + \gamma[\text{Fe}/\text{H}]$ for Milky Way, Large Magellanic Cloud and Small Magellanic Cloud Cepheids fitted together for different conditions. The slope values are the same as in Table 2.

Band	δ	γ	N	Comments
<i>V</i>	-3.252 ± 0.020	-0.048 ± 0.051	1908	Initial conditions (*)
<i>I</i>	-3.948 ± 0.020	-0.138 ± 0.051	1907	Initial conditions
<i>W_{VI}</i>	-5.005 ± 0.022	-0.251 ± 0.057	1864	Initial conditions
<i>J</i>	-4.463 ± 0.022	-0.208 ± 0.051	1196	Initial conditions
<i>H</i>	-4.748 ± 0.020	-0.152 ± 0.092	905	Initial conditions
<i>K_S</i>	-4.826 ± 0.019	-0.221 ± 0.050	1199	Initial conditions
<i>W_{JK}</i>	-5.075 ± 0.022	-0.214 ± 0.057	1198	Initial conditions
<i>V</i>	-3.274 ± 0.020	-0.084 ± 0.051	1908	Gaia EDR3 parallax ZP = $-17\mu\text{as}$
<i>I</i>	-3.966 ± 0.020	-0.165 ± 0.050	1907	Gaia EDR3 parallax ZP = $-17\mu\text{as}$
<i>W_{VI}</i>	-5.020 ± 0.022	-0.275 ± 0.058	1864	Gaia EDR3 parallax ZP = $-17\mu\text{as}$
<i>J</i>	-4.495 ± 0.022	-0.258 ± 0.052	1196	Gaia EDR3 parallax ZP = $-17\mu\text{as}$
<i>H</i>	-4.778 ± 0.020	-0.241 ± 0.099	905	Gaia EDR3 parallax ZP = $-17\mu\text{as}$
<i>K_S</i>	-4.857 ± 0.019	-0.271 ± 0.051	1199	Gaia EDR3 parallax ZP = $-17\mu\text{as}$
<i>W_{JK}</i>	-5.106 ± 0.022	-0.263 ± 0.058	1198	Gaia EDR3 parallax ZP = $-17\mu\text{as}$
<i>V</i>	-3.252 ± 0.020	-0.036 ± 0.052	1952	R=0.7° around SMC center
<i>I</i>	-3.948 ± 0.020	-0.130 ± 0.052	1951	R=0.7° around SMC center
<i>W_{VI}</i>	-5.005 ± 0.022	-0.252 ± 0.058	1908	R=0.7° around SMC center
<i>J</i>	-4.464 ± 0.022	-0.206 ± 0.052	1241	R=0.7° around SMC center
<i>K_S</i>	-4.826 ± 0.019	-0.218 ± 0.051	1244	R=0.7° around SMC center
<i>W_{JK}</i>	-5.075 ± 0.022	-0.208 ± 0.058	1242	R=0.7° around SMC center
<i>V</i>	-3.250 ± 0.020	-0.077 ± 0.051	1845	R=0.5° around SMC center
<i>I</i>	-3.947 ± 0.020	-0.160 ± 0.053	1842	R=0.5° around SMC center
<i>W_{VI}</i>	-5.005 ± 0.022	-0.251 ± 0.059	1800	R=0.5° around SMC center
<i>J</i>	-4.462 ± 0.022	-0.225 ± 0.054	1132	R=0.5° around SMC center
<i>K_S</i>	-4.825 ± 0.019	-0.234 ± 0.050	1132	R=0.5° around SMC center
<i>W_{JK}</i>	-5.075 ± 0.022	-0.222 ± 0.057	1132	R=0.5° around SMC center

NOTE—(*) Initial conditions corresponds to *Gaia* EDR3 parallaxes corrected for individual zero-point and SMC Cepheids limited to a radius of 0.6 degree around the SMC center.

Table 4. Sample of Milky Way Cepheids and main parameters. Parallaxes from *Gaia* EDR3 include zero point correction. Stars with a RUWE parameter larger than 1.4 were marked with a star and excluded from the sample. **References:** (F95): reddening from Fernie et al. (1995) multiplied by 0.94; (A12): reddening from Acharova et al. (2012); (G14): metallicity from Genovali et al. (2014); (G14b): metallicity from the literature (Genovali et al. 2013; Lemasle et al. 2007; Luck et al. 2011; Luck & Lambert 2011; Pedicelli et al. 2010; Romaniello et al. 2008; Sziládi et al. 2007; Yong et al. 2006) rescaled to Genovali et al. (2014) solar abundance; (G15): metallicity from Genovali et al. (2015).

Star	Period (day)	π_{EDR3} (mas)	RUWE	$E(B - V)$ (mag)	Ref.	[Fe/H] (dex)	Ref.
AA Gem	11.302	0.311 ± 0.018	1.25	0.345 ± 0.036	F95	-0.08 ± 0.05	G15
AC Mon	8.014	0.383 ± 0.019	1.38	0.507 ± 0.033	F95	-0.03 ± 0.06	G14b
AD Gem	3.788	0.370 ± 0.020	0.97	0.206 ± 0.048	F95	-0.14 ± 0.06	G15
AD Pup	13.596	0.254 ± 0.017	1.36	0.363 ± 0.020	F95	-0.20 ± 0.15	G14b
AE Vel	7.134	0.369 ± 0.012	0.97	0.691 ± 0.055	F95	0.14 ± 0.06	G14b
AG Cru	3.837	0.758 ± 0.020	1.02	0.242 ± 0.020	F95	0.08 ± 0.06	G14b
AP Pup	5.084	0.924 ± 0.020	1.05	0.250 ± 0.034	F95	-0.16 ± 0.15	G14b
AP Sgr	5.058	1.217 ± 0.024	0.88	0.184 ± 0.015	F95	0.10 ± 0.08	G14b
AQ Car	9.769	0.361 ± 0.016	1.07	0.168 ± 0.013	F95	-0.30 ± 0.15	G14b
AQ Pup	30.149	0.294 ± 0.023	1.18	0.531 ± 0.017	F95	0.06 ± 0.05	G15
AS Per	4.973	0.650 ± 0.016	1.08	0.684 ± 0.041	F95	0.14 ± 0.06	G14b
AT Pup	6.665	0.604 ± 0.016	1.04	0.166 ± 0.011	F95	-0.22 ± 0.15	G14b
AV Sgr	15.415	0.404 ± 0.025	0.84	1.238 ± 0.027	F95	0.35 ± 0.17	G15
AW Per	6.464	1.093 ± 0.029	1.16	0.479 ± 0.016	F95	0.04 ± 0.06	G14b
AY Cas	2.872	0.414 ± 0.019	1.07	0.760 ± 0.049	F95	0.02 ± 0.06	G14b
AY Cen	5.310	0.574 ± 0.014	0.95	0.357 ± 0.066	F95	0.08 ± 0.06	G14b
AY Sgr	6.570	0.546 ± 0.019	0.85	0.840 ± 0.009	F95	0.11 ± 0.06	G15
BB Her	7.508	0.280 ± 0.015	1.06	0.392 ± 0.039	A12	0.26 ± 0.06	G14b
BB Sgr	6.637	1.188 ± 0.024	0.82	0.285 ± 0.011	F95	0.08 ± 0.08	G14b
BE Mon	2.706	0.504 ± 0.017	1.17	0.549 ± 0.036	F95	0.05 ± 0.09	G15
BF Oph	4.068	1.189 ± 0.024	0.84	0.261 ± 0.016	F95	0.14 ± 0.06	G14b
BG Vel	6.924	1.045 ± 0.017	0.99	0.434 ± 0.011	F95	-0.10 ± 0.15	G14b
BK Aur	8.002	0.426 ± 0.015	1.01	0.393 ± 0.026	F95	-0.07 ± 0.15	G14b
BM Per	22.952	0.334 ± 0.022	0.99	0.919 ± 0.059	F95	0.23 ± 0.06	G14b
BM Pup	7.199	0.302 ± 0.013	1.18	0.575 ± 0.058	F95	-0.07 ± 0.08	G15
BN Pup	13.673	0.301 ± 0.015	1.25	0.422 ± 0.017	F95	0.03 ± 0.05	G15
BP Cas	6.273	0.442 ± 0.013	1.02	0.864 ± 0.014	F95	0.09 ± 0.06	G14b
BZ Cyg	10.142	0.500 ± 0.014	1.14	0.832 ± 0.018	F95	0.19 ± 0.08	G14b
CD Cas	7.801	0.412 ± 0.014	1.06	0.745 ± 0.012	F95	0.13 ± 0.06	G14b
CD Cyg	17.074	0.394 ± 0.016	1.01	0.512 ± 0.021	F95	0.15 ± 0.06	G14b
CE Pup	49.326	0.114 ± 0.014	0.82	0.740 ± 0.074	A12	-0.04 ± 0.09	G14
CF Cas	4.875	0.316 ± 0.012	1.04	0.556 ± 0.021	F95	0.02 ± 0.06	G14b
CG Cas	4.366	0.296 ± 0.017	1.03	0.667 ± 0.009	F95	0.09 ± 0.06	G14b
CK Sct	7.415	0.490 ± 0.020	0.97	0.816 ± 0.024	F95	0.21 ± 0.06	G14b
CN Car	4.933	0.342 ± 0.014	0.96	0.438 ± 0.049	F95	0.21 ± 0.06	G14b
CP Cep	17.859	0.279 ± 0.021	1.01	0.681 ± 0.045	F95	-0.01 ± 0.08	G14b
CR Cep	6.233	0.699 ± 0.013	1.06	0.704 ± 0.009	F95	-0.06 ± 0.08	G14b
CR Ser	5.301	0.578 ± 0.020	1.19	0.974 ± 0.017	F95	0.12 ± 0.08	G15
CS Mon	6.732	0.324 ± 0.014	1.04	0.528 ± 0.032	F95	-0.08 ± 0.06	G14b
CS Ori	3.889	0.257 ± 0.022	1.33	0.373 ± 0.030	F95	-0.25 ± 0.06	G15
CS Vel	5.905	0.272 ± 0.016	0.91	0.716 ± 0.027	F95	0.12 ± 0.06	G14b

Table 4 (continued)

Star	Period (day)	π_{EDR3} (mas)	RUWE	$E(B - V)$ (mag)	Ref.	[Fe/H] (dex)	Ref.
CV Mon	5.379	0.601 ± 0.015	1.10	0.705 ± 0.018	F95	0.09 ± 0.09	G15
CY Car	4.266	0.427 ± 0.011	0.93	0.409 ± 0.043	F95	0.11 ± 0.06	G14b
CY Cas	14.377	0.255 ± 0.019	1.07	0.952 ± 0.008	F95	0.06 ± 0.08	G14b
CZ Cas	5.664	0.292 ± 0.016	0.96	0.761 ± 0.030	F95	0.07 ± 0.06	G14b
DD Cas	9.812	0.346 ± 0.013	1.05	0.486 ± 0.016	F95	0.10 ± 0.08	G14b
DF Cas	3.832	0.374 ± 0.014	1.05	0.564 ± 0.049	F95	0.13 ± 0.08	G14b
DW Per	3.650	0.296 ± 0.019	1.31	0.620 ± 0.033	F95	-0.05 ± 0.06	G14b
EK Mon	3.958	0.376 ± 0.021	1.16	0.547 ± 0.003	F95	-0.05 ± 0.15	G14b
ER Car	7.719	0.869 ± 0.015	0.82	0.111 ± 0.016	F95	0.15 ± 0.06	G14b
EX Vel	13.234	0.204 ± 0.015	0.94	0.728 ± 0.052	F95	0.07 ± 0.06	G14b
FI Car	13.458	0.242 ± 0.019	0.99	0.694 ± 0.007	F95	0.31 ± 0.06	G14b
FM Aql	6.114	1.014 ± 0.026	1.26	0.635 ± 0.019	F95	0.24 ± 0.06	G14b
FN Aql	9.482	0.736 ± 0.025	1.12	0.486 ± 0.008	F95	-0.06 ± 0.06	G14b
GH Cyg	7.818	0.417 ± 0.014	1.07	0.608 ± 0.023	F95	0.21 ± 0.06	G14b
GI Cyg	5.783	0.273 ± 0.017	1.01	0.734 ± 0.073	F95	0.27 ± 0.06	G14b
GQ Ori	8.616	0.408 ± 0.021	0.87	0.224 ± 0.013	F95	0.20 ± 0.08	G15
GU Nor	3.453	0.565 ± 0.015	0.87	0.683 ± 0.029	F95	0.08 ± 0.06	G15
GX Car	7.197	0.459 ± 0.013	1.02	0.380 ± 0.008	F95	0.14 ± 0.06	G14b
GY Sge	51.790	0.342 ± 0.023	0.95	1.183 ± 0.111	F95	0.29 ± 0.06	G14b
HW Car	9.199	0.397 ± 0.012	0.94	0.181 ± 0.018	F95	0.09 ± 0.06	G14b
IQ Nor	8.220	0.535 ± 0.018	0.97	0.676 ± 0.044	F95	0.22 ± 0.07	G15
IT Car	7.533	0.702 ± 0.020	1.08	0.212 ± 0.016	F95	0.14 ± 0.06	G14b
KK Cen	12.180	0.152 ± 0.018	1.03	0.555 ± 0.033	F95	0.24 ± 0.06	G14b
KN Cen	34.020	0.251 ± 0.018	1.03	0.728 ± 0.040	F95	0.55 ± 0.12	G15
KQ Sco	28.705	0.472 ± 0.021	0.91	0.852 ± 0.041	F95	0.52 ± 0.08	G15
LS Pup	14.147	0.214 ± 0.016	1.25	0.452 ± 0.009	F95	-0.12 ± 0.11	G15
MW Cyg	5.955	0.542 ± 0.019	1.21	0.651 ± 0.039	F95	0.09 ± 0.08	G14b
MZ Cen	10.354	0.221 ± 0.017	0.84	0.782 ± 0.077	F95	0.27 ± 0.10	G15
QY Cen	17.752	0.293 ± 0.021	1.02	1.213 ± 0.216	F95	0.24 ± 0.06	G14b
R Cru	5.826	1.078 ± 0.028	1.16	0.156 ± 0.012	F95	0.13 ± 0.06	G14b
R Mus	7.510	1.076 ± 0.018	1.07	0.149 ± 0.030	F95	-0.08 ± 0.06	G14b
R TrA	3.389	1.560 ± 0.016	0.89	0.167 ± 0.025	F95	0.19 ± 0.06	G14b
RR Lac	6.416	0.424 ± 0.015	1.10	0.267 ± 0.023	F95	0.04 ± 0.06	G14b
RS Nor	6.198	0.472 ± 0.017	0.94	0.577 ± 0.036	F95	0.18 ± 0.08	G15
RS Ori	7.567	0.589 ± 0.030	1.12	0.332 ± 0.010	F95	0.11 ± 0.09	G15
RS Pup	41.480	0.581 ± 0.017	1.16	0.451 ± 0.010	F95	0.07 ± 0.15	G14b
RU Sct	19.704	0.526 ± 0.024	0.87	0.914 ± 0.017	F95	0.14 ± 0.04	G15
RV Sco	6.061	1.257 ± 0.021	0.81	0.343 ± 0.007	F95	0.11 ± 0.06	G14b
RW Cas	14.795	0.335 ± 0.019	1.26	0.440 ± 0.032	F95	0.22 ± 0.08	G14b
RX Aur	11.624	0.654 ± 0.021	0.98	0.254 ± 0.020	F95	0.10 ± 0.06	G14b
RY CMa	4.678	0.825 ± 0.029	1.29	0.238 ± 0.016	F95	0.00 ± 0.15	G14b
RY Sco	20.323	0.764 ± 0.032	0.73	0.654 ± 0.044	F95	0.01 ± 0.06	G15
RY Vel	28.136	0.376 ± 0.021	1.07	0.539 ± 0.012	F95	-0.05 ± 0.15	G14b
RZ Vel	20.398	0.661 ± 0.017	1.24	0.301 ± 0.011	F95	0.05 ± 0.15	G14b
S Cru	4.690	1.342 ± 0.024	0.94	0.172 ± 0.014	F95	0.11 ± 0.06	G14b
S Nor	9.754	1.099 ± 0.022	0.88	0.182 ± 0.008	F95	0.02 ± 0.09	G14b
S TrA	6.324	1.120 ± 0.022	1.04	0.086 ± 0.010	F95	0.21 ± 0.06	G14b

Table 4 (continued)

Star	Period (day)	π_{EDR3} (mas)	RUWE	$E(B - V)$ (mag)	Ref.	[Fe/H] (dex)	Ref.
SS CMa	12.361	0.307 ± 0.013	1.11	0.551 ± 0.012	F95	0.06 ± 0.04	G15
SS Sct	3.671	0.934 ± 0.023	0.84	0.340 ± 0.022	F95	0.14 ± 0.06	G14b
ST Tau	4.034	0.916 ± 0.034	1.35	0.328 ± 0.006	F95	-0.14 ± 0.15	G14b
ST Vel	5.858	0.384 ± 0.015	1.19	0.530 ± 0.024	F95	-0.14 ± 0.15	G14b
SV Mon	15.233	0.464 ± 0.032	1.01	0.264 ± 0.021	F95	0.12 ± 0.08	G15
SV Vel	14.097	0.434 ± 0.018	1.02	0.376 ± 0.024	F95	0.12 ± 0.06	G14b
SV Vul	44.993	0.402 ± 0.021	1.20	0.474 ± 0.024	F95	0.05 ± 0.08	G14b
SW Cas	5.441	0.461 ± 0.012	1.12	0.475 ± 0.027	F95	-0.03 ± 0.08	G14b
SW Vel	23.407	0.413 ± 0.018	1.05	0.338 ± 0.009	F95	-0.15 ± 0.15	G14b
SX Car	4.860	0.515 ± 0.022	1.25	0.323 ± 0.026	F95	0.05 ± 0.06	G14b
SX Per	4.290	0.313 ± 0.019	1.19	0.537 ± 0.046	F95	-0.03 ± 0.06	G14b
SX Vel	9.550	0.501 ± 0.019	1.02	0.237 ± 0.014	F95	-0.18 ± 0.15	G14b
SY Aur	10.145	0.462 ± 0.020	1.08	0.386 ± 0.040	F95	-0.07 ± 0.15	G14b
SZ Aql	17.141	0.525 ± 0.020	0.94	0.553 ± 0.022	F95	0.18 ± 0.08	G14b
SZ Cas	13.639	0.407 ± 0.017	1.01	0.713 ± 0.060	F95	0.07 ± 0.06	G14b
SZ Cyg	15.110	0.445 ± 0.012	0.96	0.594 ± 0.004	F95	0.09 ± 0.08	G14b
T Ant	5.898	0.312 ± 0.014	1.18	0.300 ± 0.030	A12	-0.20 ± 0.06	G14b
T Cru	6.733	1.222 ± 0.014	0.82	0.191 ± 0.022	F95	0.14 ± 0.06	G14b
T Vel	4.640	0.940 ± 0.016	0.93	0.282 ± 0.018	F95	-0.02 ± 0.15	G14b
T Vul	4.435	1.719 ± 0.058	1.20	0.092 ± 0.017	F95	0.01 ± 0.08	G14b
TT Aql	13.755	0.997 ± 0.023	1.08	0.487 ± 0.024	F95	0.22 ± 0.06	G14b
TV CMa	4.670	0.420 ± 0.015	1.20	0.574 ± 0.029	F95	0.01 ± 0.07	G15
TV Cam	5.295	0.237 ± 0.018	1.11	0.560 ± 0.023	F95	0.04 ± 0.06	G14b
TW CMa	6.995	0.384 ± 0.019	1.15	0.374 ± 0.033	F95	0.04 ± 0.09	G15
TW Nor	10.786	0.360 ± 0.020	0.89	1.190 ± 0.023	F95	0.27 ± 0.10	G15
TX Cen	17.098	0.332 ± 0.018	0.94	0.941 ± 0.038	F95	0.44 ± 0.12	G15
TX Cyg	14.710	0.829 ± 0.019	0.95	1.123 ± 0.005	F95	0.20 ± 0.08	G14b
TY Sct	11.053	0.371 ± 0.016	0.91	0.930 ± 0.017	F95	0.37 ± 0.06	G14b
TZ Mon	7.428	0.298 ± 0.015	1.24	0.434 ± 0.023	F95	-0.02 ± 0.07	G15
TZ Mus	4.945	0.266 ± 0.020	1.00	0.676 ± 0.020	F95	0.10 ± 0.06	G14b
U Car	38.829	0.561 ± 0.023	1.23	0.276 ± 0.013	F95	0.17 ± 0.09	G14b
U Nor	12.644	0.625 ± 0.019	0.98	0.868 ± 0.038	F95	0.07 ± 0.09	G14b
U Sgr	6.745	1.605 ± 0.023	0.85	0.408 ± 0.007	F95	0.08 ± 0.08	G14b
UU Mus	11.636	0.306 ± 0.012	1.01	0.431 ± 0.041	F95	0.11 ± 0.09	G14b
UX Car	3.682	0.653 ± 0.019	1.02	0.102 ± 0.023	F95	-0.10 ± 0.15	G14b
UX Per	4.566	0.162 ± 0.020	1.17	0.462 ± 0.024	F95	-0.05 ± 0.06	G14b
UY Car	5.544	0.455 ± 0.014	0.94	0.188 ± 0.017	F95	0.13 ± 0.06	G14b
UY Per	5.365	0.415 ± 0.015	1.17	0.888 ± 0.013	F95	0.18 ± 0.06	G14b
UZ Car	5.205	0.401 ± 0.013	0.95	0.213 ± 0.034	F95	0.13 ± 0.06	G14b
UZ Cas	4.259	0.251 ± 0.020	1.23	0.469 ± 0.034	F95	-0.05 ± 0.06	G14b
UZ Sct	14.744	0.324 ± 0.025	0.91	0.959 ± 0.023	F95	0.33 ± 0.08	G15
V Car	6.697	0.797 ± 0.014	1.04	0.164 ± 0.013	F95	-0.06 ± 0.15	G14b
V Cen	5.494	1.409 ± 0.022	1.06	0.265 ± 0.016	F95	0.04 ± 0.09	G14b
V Lac	4.983	0.496 ± 0.016	1.09	0.293 ± 0.034	F95	0.06 ± 0.06	G14b
V Vel	4.371	0.953 ± 0.017	1.03	0.225 ± 0.021	F95	-0.30 ± 0.15	G14b
V0339 Cen	9.466	0.568 ± 0.021	0.89	0.426 ± 0.016	F95	0.06 ± 0.03	G15
V0340 Ara	20.814	0.239 ± 0.020	0.93	0.548 ± 0.008	F95	0.33 ± 0.09	G15

Table 4 (continued)

Star	Period (day)	π_{EDR3} (mas)	RUWE	$E(B - V)$ (mag)	Ref.	[Fe/H] (dex)	Ref.
V0340 Nor	11.289	0.491 ± 0.025	0.92	0.312 ± 0.050	F95	0.07 ± 0.07	G15
V0378 Cen	6.460	0.524 ± 0.019	0.99	0.374 ± 0.049	F95	0.08 ± 0.06	G14b
V0381 Cen	5.079	0.818 ± 0.020	1.06	0.206 ± 0.013	F95	0.02 ± 0.06	G14b
V0386 Cyg	5.258	0.894 ± 0.013	0.95	0.907 ± 0.033	F95	0.11 ± 0.08	G14b
V0402 Cyg	4.365	0.410 ± 0.011	0.92	0.455 ± 0.062	F95	0.02 ± 0.08	G14b
V0459 Cyg	7.251	0.382 ± 0.014	1.09	0.775 ± 0.024	F95	0.09 ± 0.06	G14b
V0470 Sco	16.261	0.534 ± 0.029	0.97	1.550 ± 0.124	F95	0.16 ± 0.06	G15
V0493 Aql	2.988	0.472 ± 0.017	1.12	0.730 ± 0.087	F95	0.03 ± 0.06	G14b
V0496 Cen	4.424	0.563 ± 0.013	0.94	0.579 ± 0.031	F95	0.09 ± 0.06	G14b
V0520 Cyg	4.049	0.437 ± 0.012	1.03	0.754 ± 0.075	F95	0.08 ± 0.06	G14b
V0538 Cyg	6.119	0.394 ± 0.017	0.99	0.656 ± 0.021	F95	0.05 ± 0.06	G14b
V0600 Aql	7.239	0.523 ± 0.019	1.13	0.812 ± 0.007	F95	0.03 ± 0.08	G14b
V0609 Cyg	31.088	0.295 ± 0.017	1.12	1.243 ± 0.124	F95	0.22 ± 0.06	G14b
V0636 Cas	8.377	1.372 ± 0.018	1.02	0.593 ± 0.065	F95	0.07 ± 0.08	G14b
V0636 Sco	6.797	1.180 ± 0.034	1.15	0.227 ± 0.017	F95	0.10 ± 0.06	G14b
V0733 Aql	6.179	0.244 ± 0.015	0.98	0.106 ± 0.011	A12	0.08 ± 0.08	G14b
V0737 Cen	7.066	1.213 ± 0.019	0.92	0.227 ± 0.022	F95	0.14 ± 0.06	G14b
V1154 Cyg	4.925	0.442 ± 0.012	1.04	0.315 ± 0.031	F95	-0.10 ± 0.08	G14b
V1162 Aql	5.376	0.823 ± 0.023	0.95	0.184 ± 0.011	F95	0.01 ± 0.08	G14b
VW Cen	15.036	0.260 ± 0.016	1.06	0.424 ± 0.022	F95	0.41 ± 0.08	G15
VW Cru	5.265	0.738 ± 0.016	0.85	0.640 ± 0.046	F95	0.19 ± 0.06	G14b
VY Car	18.890	0.565 ± 0.017	0.92	0.270 ± 0.019	F95	-0.06 ± 0.15	G14b
VY Cyg	7.857	0.485 ± 0.012	1.07	0.596 ± 0.021	F95	0.00 ± 0.08	G14b
VY Per	5.532	0.485 ± 0.017	1.15	0.948 ± 0.018	F95	0.04 ± 0.06	G14b
VY Sgr	13.557	0.412 ± 0.025	0.81	0.903 ± 0.243	F95	0.33 ± 0.12	G15
VZ Cyg	4.864	0.545 ± 0.016	1.31	0.291 ± 0.015	F95	0.05 ± 0.08	G14b
VZ Pup	23.175	0.220 ± 0.015	1.24	0.433 ± 0.018	F95	-0.01 ± 0.04	G15
W Gem	7.914	1.006 ± 0.028	1.23	0.264 ± 0.011	F95	0.02 ± 0.06	G14b
WW Pup	5.517	0.212 ± 0.016	1.14	0.334 ± 0.017	F95	0.13 ± 0.16	G15
WX Pup	8.937	0.387 ± 0.015	1.06	0.306 ± 0.018	F95	-0.15 ± 0.15	G14b
WY Pup	5.251	0.258 ± 0.013	1.02	0.259 ± 0.031	F95	-0.10 ± 0.08	G15
WZ Pup	5.027	0.281 ± 0.017	1.35	0.196 ± 0.022	F95	-0.07 ± 0.06	G15
WZ Sgr	21.851	0.612 ± 0.028	0.94	0.457 ± 0.025	F95	0.28 ± 0.08	G15
X Cru	6.220	0.654 ± 0.019	0.95	0.294 ± 0.019	F95	0.15 ± 0.06	G14b
X Cyg	16.386	0.910 ± 0.020	1.28	0.251 ± 0.010	F95	0.10 ± 0.08	G14b
X Pup	25.973	0.397 ± 0.020	1.04	0.396 ± 0.015	F95	0.02 ± 0.08	G15
X Sct	4.198	0.634 ± 0.019	0.80	0.581 ± 0.030	F95	0.12 ± 0.09	G15
X Sgr	7.013	2.843 ± 0.141	1.22	0.189 ± 0.020	F95	-0.21 ± 0.30	G14b
X Vul	6.320	0.864 ± 0.022	1.06	0.775 ± 0.021	F95	0.07 ± 0.08	G14b
XX Cen	10.953	0.570 ± 0.026	1.24	0.245 ± 0.012	F95	0.04 ± 0.09	G14b
XX Mon	5.456	0.242 ± 0.013	0.86	0.586 ± 0.014	F95	0.01 ± 0.08	G15
XX Sgr	6.424	0.724 ± 0.027	1.10	0.493 ± 0.016	F95	-0.01 ± 0.06	G15
XX Vel	6.985	0.308 ± 0.013	0.88	0.530 ± 0.007	F95	0.11 ± 0.06	G14b
XZ Car	16.651	0.473 ± 0.018	1.05	0.372 ± 0.026	F95	0.19 ± 0.06	G14b
Y Aur	3.859	0.541 ± 0.017	1.12	0.384 ± 0.031	F95	-0.26 ± 0.15	G14b
Y Lac	4.324	0.431 ± 0.013	1.05	0.212 ± 0.020	F95	0.03 ± 0.06	G14b
Y Oph	17.125	1.348 ± 0.036	1.03	0.606 ± 0.030	F95	0.06 ± 0.08	G14b

Table 4 (continued)

Star	Period (day)	π_{EDR3} (mas)	RUWE	$E(B - V)$ (mag)	Ref.	[Fe/H] (dex)	Ref.
Y Sct	10.342	0.558 ± 0.020	0.94	0.792 ± 0.021	F95	0.23 ± 0.06	G14b
YZ Aur	18.193	0.233 ± 0.016	0.99	0.548 ± 0.055	F95	-0.33 ± 0.15	G14b
YZ Car	18.168	0.358 ± 0.018	1.17	0.324 ± 0.039	F95	0.00 ± 0.06	G14b
YZ Sgr	9.554	0.860 ± 0.024	0.95	0.289 ± 0.007	F95	0.06 ± 0.08	G14b
Z Lac	10.886	0.510 ± 0.021	1.05	0.352 ± 0.015	F95	0.10 ± 0.06	G14b
Z Sct	12.901	0.357 ± 0.018	0.90	0.535 ± 0.039	F95	0.12 ± 0.09	G15

Table 5. Optical and NIR mean apparent magnitudes for the sample of Milky Way Cepheids. The magnitudes do not include the reddening correction. The uncertainties are only the random errors and do not include photometric zero point errors. **References:** (B97): Barnes et al. (1997); (F08): Feast et al. (2008); (L92): Laney & Stobie (1992); (M11): Monson & Pierce (2011); (W84): Welch et al. (1984). All magnitudes in V and I are from Berdnikov (2008).

Star	V (mag)	I (mag)	J (mag)	H (mag)	K_S (mag)	Ref. NIR
AA Gem	9.735 ± 0.008	—	7.647 ± 0.011	7.206 ± 0.010	7.069 ± 0.020	M11
AC Mon	10.100 ± 0.016	8.708 ± 0.012	7.590 ± 0.013	7.072 ± 0.011	6.867 ± 0.012	M11
AD Gem	—	—	8.453 ± 0.006	8.154 ± 0.006	8.043 ± 0.007	B97, M11
AD Pup	9.898 ± 0.006	8.716 ± 0.006	—	—	—	—
AE Vel	10.257 ± 0.009	8.730 ± 0.007	—	—	—	—
AG Cru	8.228 ± 0.006	7.346 ± 0.006	—	—	—	—
AP Pup	7.385 ± 0.006	6.463 ± 0.006	—	—	—	—
AP Sgr	6.967 ± 0.006	6.053 ± 0.006	—	—	—	—
AQ Car	8.892 ± 0.023	7.895 ± 0.020	—	—	—	—
AQ Pup	8.690 ± 0.006	7.153 ± 0.006	6.000 ± 0.006	5.484 ± 0.008	5.256 ± 0.009	L92
AS Per	—	—	6.941 ± 0.014	6.482 ± 0.007	6.279 ± 0.017	M11
AT Pup	7.985 ± 0.006	7.080 ± 0.006	—	—	—	—
AV Sgr	11.331 ± 0.021	8.851 ± 0.013	—	—	—	—
AW Per	7.473 ± 0.140	—	5.222 ± 0.010	4.836 ± 0.009	4.676 ± 0.010	M11
AX Cir	5.887 ± 0.006	4.987 ± 0.006	—	—	—	—
AY Cas	11.543 ± 0.024	—	—	—	—	—
AY Cen	8.818 ± 0.006	7.701 ± 0.006	—	—	—	—
AY Sgr	10.559 ± 0.012	8.729 ± 0.009	7.140 ± 0.008	6.534 ± 0.010	6.282 ± 0.016	M11
BB Her	10.093 ± 0.007	8.941 ± 0.010	—	—	—	—
BB Sgr	6.952 ± 0.006	5.848 ± 0.006	5.025 ± 0.006	4.643 ± 0.007	4.496 ± 0.008	L92, W84
BE Mon	10.574 ± 0.008	9.243 ± 0.008	8.265 ± 0.014	7.857 ± 0.011	7.701 ± 0.024	M11
BF Oph	7.342 ± 0.006	6.367 ± 0.006	5.626 ± 0.008	5.298 ± 0.007	5.147 ± 0.009	L92, W84
BG Lac	8.897 ± 0.006	7.811 ± 0.014	7.023 ± 0.006	6.655 ± 0.006	6.500 ± 0.006	B97, M11
BG Vel	7.653 ± 0.006	6.342 ± 0.006	—	—	—	—
BK Aur	9.445 ± 0.015	—	7.300 ± 0.015	6.890 ± 0.019	6.735 ± 0.021	M11
BM Per	10.428 ± 0.028	—	6.680 ± 0.015	6.007 ± 0.012	5.724 ± 0.018	M11
BM Pup	10.846 ± 0.006	9.414 ± 0.006	—	—	—	—
BN Pup	9.907 ± 0.016	8.585 ± 0.020	7.534 ± 0.008	7.079 ± 0.009	6.880 ± 0.008	L92
BP Cas	10.951 ± 0.021	—	—	—	—	—
BZ Cyg	10.221 ± 0.006	8.327 ± 0.018	6.774 ± 0.014	6.153 ± 0.010	5.879 ± 0.014	M11
β Dor	3.737 ± 0.006	2.939 ± 0.006	2.365 ± 0.006	2.038 ± 0.006	1.925 ± 0.006	F08, L92
CD Cas	10.782 ± 0.009	—	7.644 ± 0.006	7.093 ± 0.012	6.878 ± 0.012	M11
CD Cyg	8.963 ± 0.009	7.498 ± 0.028	6.363 ± 0.015	5.853 ± 0.012	5.668 ± 0.011	W84, M11
CE Pup	11.832 ± 0.010	9.968 ± 0.007	—	—	—	—
CF Cas	11.138 ± 0.006	9.756 ± 0.012	8.606 ± 0.010	8.136 ± 0.012	7.923 ± 0.012	W84, M11
CG Cas	11.378 ± 0.010	—	—	—	—	—
CK Sct	—	—	7.393 ± 0.006	6.822 ± 0.010	6.610 ± 0.014	M11
CN Car	10.684 ± 0.008	9.355 ± 0.009	—	—	—	—
CP Cep	10.588 ± 0.012	8.766 ± 0.024	7.348 ± 0.010	6.726 ± 0.012	6.492 ± 0.012	M11
CR Cep	9.646 ± 0.008	7.979 ± 0.020	6.654 ± 0.006	6.101 ± 0.007	5.890 ± 0.007	M11
CR Ser	10.857 ± 0.009	8.899 ± 0.026	7.353 ± 0.007	6.763 ± 0.007	6.503 ± 0.012	M11
CS Mon	11.005 ± 0.006	9.651 ± 0.006	—	—	—	—
CS Ori	11.399 ± 0.037	10.261 ± 0.019	9.341 ± 0.011	8.960 ± 0.009	8.810 ± 0.017	M11
CS Vel	11.702 ± 0.007	10.069 ± 0.007	8.735 ± 0.010	8.228 ± 0.014	7.973 ± 0.011	L92, W84

Table 5 (continued)

Star	V (mag)	I (mag)	J (mag)	H (mag)	K_S (mag)	Ref. NIR
CV Mon	10.291 ± 0.006	8.645 ± 0.006	7.323 ± 0.011	6.790 ± 0.007	6.545 ± 0.007	L92, W84, M11
CY Car	9.755 ± 0.007	8.712 ± 0.006	—	—	—	—
CY Cas	11.643 ± 0.020	—	7.876 ± 0.028	7.180 ± 0.018	6.915 ± 0.023	M11
CZ Cas	11.752 ± 0.009	10.059 ± 0.021	—	—	—	—
DD Cas	9.888 ± 0.007	8.561 ± 0.025	7.537 ± 0.008	7.073 ± 0.011	6.909 ± 0.014	M11
DF Cas	10.879 ± 0.006	—	—	—	—	—
DL Cas	8.971 ± 0.006	—	6.560 ± 0.014	6.106 ± 0.011	5.912 ± 0.015	W84, M11
DW Per	11.577 ± 0.008	—	—	—	—	—
δ Cep	3.930 ± 0.010	—	2.676 ± 0.006	2.393 ± 0.006	2.291 ± 0.006	F08, B97
EK Mon	11.062 ± 0.006	9.617 ± 0.006	—	—	—	—
ER Car	6.828 ± 0.006	5.961 ± 0.006	—	—	—	—
EX Vel	11.573 ± 0.007	9.775 ± 0.006	—	—	—	—
EY Car	10.359 ± 0.010	9.260 ± 0.008	—	—	—	—
Eta Aql	3.878 ± 0.006	3.024 ± 0.006	2.386 ± 0.006	2.067 ± 0.006	1.951 ± 0.006	B97, W84
FI Car	11.626 ± 0.010	9.855 ± 0.009	—	—	—	—
FM Aql	8.278 ± 0.006	6.780 ± 0.010	5.681 ± 0.006	5.217 ± 0.006	5.026 ± 0.006	B97, W84, M11
FN Aql	8.383 ± 0.006	6.992 ± 0.006	5.965 ± 0.006	5.495 ± 0.006	5.315 ± 0.006	B97, W84, M11
FN Vel	10.303 ± 0.006	8.830 ± 0.007	—	—	—	—
GH Cyg	9.904 ± 0.006	8.432 ± 0.011	7.262 ± 0.011	6.804 ± 0.006	6.598 ± 0.016	M11
GI Cyg	11.745 ± 0.012	—	—	—	—	—
GQ Ori	8.965 ± 0.011	7.885 ± 0.007	—	—	—	—
GU Nor	10.354 ± 0.006	8.799 ± 0.007	—	—	—	—
GX Car	9.344 ± 0.009	8.137 ± 0.006	—	—	—	—
GY Sge	10.163 ± 0.006	—	5.604 ± 0.008	4.887 ± 0.007	4.546 ± 0.006	L92, W84
HW Car	9.136 ± 0.006	8.028 ± 0.006	—	—	—	—
IQ Nor	9.665 ± 0.019	8.115 ± 0.020	—	—	—	—
IT Car	8.102 ± 0.006	7.070 ± 0.006	—	—	—	—
KK Cen	11.452 ± 0.036	9.934 ± 0.026	—	—	—	—
KN Cen	9.865 ± 0.006	7.994 ± 0.006	6.399 ± 0.007	5.747 ± 0.008	5.440 ± 0.006	L92
KQ Sco	9.835 ± 0.006	7.659 ± 0.006	5.909 ± 0.012	5.215 ± 0.010	4.901 ± 0.013	L92, W84
ℓ Car	3.723 ± 0.006	2.554 ± 0.006	1.679 ± 0.006	1.218 ± 0.006	1.054 ± 0.006	L92
LS Pup	10.462 ± 0.007	9.073 ± 0.008	7.999 ± 0.006	7.521 ± 0.007	7.312 ± 0.006	L92
MW Cyg	9.483 ± 0.006	—	6.700 ± 0.006	6.209 ± 0.009	5.998 ± 0.014	M11
MZ Cen	11.553 ± 0.007	9.786 ± 0.010	—	—	—	—
QY Cen	11.784 ± 0.006	9.350 ± 0.007	—	—	—	—
R Cru	6.771 ± 0.006	5.901 ± 0.006	—	—	—	—
R Mus	6.313 ± 0.006	5.497 ± 0.006	—	—	—	—
R TrA	6.656 ± 0.006	5.843 ± 0.006	—	—	—	—
RR Lac	8.846 ± 0.006	7.814 ± 0.015	6.977 ± 0.008	6.628 ± 0.010	6.488 ± 0.011	M11
RS Nor	10.019 ± 0.018	8.541 ± 0.013	—	—	—	—
RS Ori	8.410 ± 0.011	7.282 ± 0.012	6.408 ± 0.016	6.027 ± 0.017	5.880 ± 0.019	M11
RS Pup	7.008 ± 0.006	5.478 ± 0.006	4.341 ± 0.009	3.830 ± 0.007	3.605 ± 0.008	L92, W84
RT Aur	5.469 ± 0.076	4.811 ± 0.043	4.236 ± 0.008	3.998 ± 0.007	3.906 ± 0.006	B97, M11
RU Sct	—	—	5.909 ± 0.008	5.298 ± 0.007	5.036 ± 0.009	L92, W84, M11
RV Sco	7.046 ± 0.006	5.907 ± 0.006	—	—	—	—
RW Cam	8.657 ± 0.010	—	5.828 ± 0.012	5.291 ± 0.013	5.093 ± 0.010	M11
RW Cas	9.248 ± 0.019	7.871 ± 0.020	6.841 ± 0.024	6.372 ± 0.011	6.194 ± 0.026	M11

Table 5 (continued)

Star	V (mag)	I (mag)	J (mag)	H (mag)	K_S (mag)	Ref. NIR
RX Aur	7.670 ± 0.007	—	5.737 ± 0.008	5.363 ± 0.011	5.233 ± 0.017	M11
RX Cam	7.670 ± 0.012	—	5.178 ± 0.023	4.732 ± 0.020	4.561 ± 0.012	M11
RY CMa	8.109 ± 0.006	7.133 ± 0.006	—	—	—	—
RY Sco	7.999 ± 0.006	6.253 ± 0.006	4.899 ± 0.006	4.368 ± 0.006	4.102 ± 0.007	L92, W84
RY Vel	8.376 ± 0.006	6.827 ± 0.006	5.604 ± 0.008	5.124 ± 0.007	4.886 ± 0.006	L92, W84
RZ CMa	9.702 ± 0.007	8.504 ± 0.007	—	—	—	—
RZ Gem	10.048 ± 0.249	—	7.612 ± 0.010	7.169 ± 0.009	6.970 ± 0.015	M11
RZ Vel	7.089 ± 0.006	5.862 ± 0.006	4.889 ± 0.012	4.463 ± 0.007	4.267 ± 0.006	L92
S Cru	6.601 ± 0.006	5.732 ± 0.006	—	—	—	—
S Mus	6.133 ± 0.006	5.199 ± 0.006	4.473 ± 0.006	4.135 ± 0.006	3.983 ± 0.008	L92, W84
S Nor	6.427 ± 0.006	5.428 ± 0.006	4.652 ± 0.006	4.286 ± 0.006	4.131 ± 0.008	L92, W84
S Sge	5.612 ± 0.006	4.772 ± 0.010	4.155 ± 0.006	3.847 ± 0.006	3.732 ± 0.006	W84, B97
S TrA	6.391 ± 0.006	5.592 ± 0.006	—	—	—	—
SS CMa	—	8.480 ± 0.010	—	—	—	—
SS Sct	—	—	6.299 ± 0.008	5.938 ± 0.006	5.807 ± 0.008	W84, M11
ST Tau	8.243 ± 0.014	7.171 ± 0.016	—	—	—	—
ST Vel	9.699 ± 0.006	8.286 ± 0.006	—	—	—	—
SU Cyg	6.855 ± 0.007	6.198 ± 0.013	5.638 ± 0.007	5.397 ± 0.007	5.295 ± 0.008	W84, M11
SV Mon	8.266 ± 0.008	7.139 ± 0.006	6.262 ± 0.015	5.835 ± 0.010	5.691 ± 0.017	M11
SV Per	8.977 ± 0.011	—	6.802 ± 0.021	6.360 ± 0.016	6.198 ± 0.018	M11
SV Vel	8.583 ± 0.006	7.329 ± 0.006	—	—	—	—
SV Vul	7.216 ± 0.006	5.697 ± 0.009	4.571 ± 0.006	4.077 ± 0.006	3.887 ± 0.006	W84, L92, B97, M11
SW Cas	9.713 ± 0.007	8.438 ± 0.020	7.412 ± 0.009	6.987 ± 0.013	6.820 ± 0.015	M11
SW Vel	8.137 ± 0.014	6.850 ± 0.008	5.852 ± 0.018	5.407 ± 0.012	5.203 ± 0.011	L92
SX Car	9.082 ± 0.006	8.039 ± 0.006	—	—	—	—
SX Per	11.223 ± 0.104	—	8.769 ± 0.010	8.352 ± 0.007	8.187 ± 0.013	M11
SX Vel	8.278 ± 0.006	7.262 ± 0.006	6.474 ± 0.006	6.127 ± 0.006	5.965 ± 0.006	L92
SY Aur	9.069 ± 0.009	—	6.923 ± 0.009	6.530 ± 0.012	6.367 ± 0.014	M11
SY Nor	9.520 ± 0.023	7.949 ± 0.030	—	—	—	—
SZ Aql	8.636 ± 0.011	7.082 ± 0.015	5.865 ± 0.008	5.351 ± 0.006	5.138 ± 0.006	B97, W84, L92, M11
SZ Cas	9.843 ± 0.006	8.110 ± 0.008	—	—	—	—
SZ Cyg	9.435 ± 0.011	7.798 ± 0.026	6.530 ± 0.009	5.960 ± 0.007	5.732 ± 0.014	M11
T Ant	9.331 ± 0.006	8.523 ± 0.006	—	—	—	—
T Cru	6.570 ± 0.006	5.608 ± 0.006	—	—	—	—
T Mon	6.138 ± 0.006	4.987 ± 0.006	4.092 ± 0.009	3.648 ± 0.009	3.487 ± 0.008	W84, L92, M11
T Vel	8.029 ± 0.006	6.964 ± 0.006	6.143 ± 0.006	5.775 ± 0.006	5.605 ± 0.006	L92
T Vul	5.750 ± 0.006	5.077 ± 0.015	4.532 ± 0.006	4.272 ± 0.006	4.174 ± 0.006	W84, B97
TT Aql	7.141 ± 0.006	5.732 ± 0.009	4.671 ± 0.009	4.194 ± 0.007	4.017 ± 0.006	W84, M11, B97
TV CMa	10.587 ± 0.011	9.173 ± 0.011	8.035 ± 0.008	7.588 ± 0.011	7.386 ± 0.014	M11
TV Cam	11.729 ± 0.018	—	—	—	—	—
TW CMa	9.573 ± 0.007	8.458 ± 0.007	7.577 ± 0.010	7.183 ± 0.009	7.029 ± 0.017	M11
TW Nor	11.670 ± 0.007	9.306 ± 0.010	7.406 ± 0.022	6.705 ± 0.013	6.358 ± 0.029	L92, W84
TX Cen	10.527 ± 0.006	8.618 ± 0.006	—	—	—	—
TX Cyg	9.490 ± 0.012	7.225 ± 0.030	5.342 ± 0.020	4.633 ± 0.018	4.323 ± 0.018	M11
TX Mon	10.960 ± 0.010	9.634 ± 0.008	8.581 ± 0.013	8.121 ± 0.013	7.943 ± 0.017	M11
TY Sct	10.821 ± 0.013	8.811 ± 0.016	7.247 ± 0.011	6.637 ± 0.009	6.386 ± 0.021	M11
TZ Mon	10.793 ± 0.008	9.472 ± 0.006	8.458 ± 0.012	8.009 ± 0.014	7.815 ± 0.016	M11

Table 5 (continued)

Star	V (mag)	I (mag)	J (mag)	H (mag)	K_S (mag)	Ref. NIR
TZ Mus	11.690 ± 0.006	10.144 ± 0.008	—	—	—	—
U Aql	6.432 ± 0.006	5.271 ± 0.010	4.389 ± 0.012	3.999 ± 0.009	3.844 ± 0.010	W84, M11
U Car	6.284 ± 0.006	5.052 ± 0.006	4.104 ± 0.007	3.674 ± 0.006	3.483 ± 0.006	L92, W84
U Nor	—	—	5.825 ± 0.006	5.236 ± 0.006	4.944 ± 0.006	L92
U Sgr	6.697 ± 0.006	5.436 ± 0.006	4.512 ± 0.006	4.100 ± 0.006	3.933 ± 0.007	W84, L92, M11
U Vul	7.122 ± 0.006	5.602 ± 0.011	4.528 ± 0.009	4.093 ± 0.007	3.912 ± 0.006	B97, M11
UU Mus	—	—	7.439 ± 0.007	6.994 ± 0.006	6.788 ± 0.006	L92
UW Car	9.424 ± 0.008	8.218 ± 0.013	—	—	—	—
UX Car	8.295 ± 0.006	7.554 ± 0.006	—	—	—	—
UX Per	11.650 ± 0.018	—	—	—	—	—
UY Car	8.948 ± 0.006	8.007 ± 0.010	—	—	—	—
UY Per	11.319 ± 0.013	9.493 ± 0.016	—	—	—	—
UZ Car	9.327 ± 0.006	8.365 ± 0.006	—	—	—	—
UZ Cas	11.379 ± 0.007	—	—	—	—	—
UZ Sct	11.289 ± 0.022	9.148 ± 0.035	7.418 ± 0.010	6.741 ± 0.010	6.485 ± 0.016	M11
V Car	7.368 ± 0.006	6.433 ± 0.006	5.728 ± 0.006	5.396 ± 0.006	5.249 ± 0.006	L92
V Cen	6.830 ± 0.006	5.794 ± 0.006	4.995 ± 0.006	4.638 ± 0.006	4.479 ± 0.009	L92, W84
V Lac	8.932 ± 0.007	—	—	—	—	—
V Vel	7.586 ± 0.006	6.691 ± 0.006	—	—	—	—
V0339 Cen	8.714 ± 0.013	7.384 ± 0.010	—	—	—	—
V0340 Ara	10.228 ± 0.014	8.580 ± 0.007	—	—	—	—
V0340 Nor	8.403 ± 0.008	7.167 ± 0.008	—	—	—	—
V0350 Sgr	7.481 ± 0.006	6.435 ± 0.006	5.627 ± 0.011	5.256 ± 0.011	5.130 ± 0.008	W84
V0378 Cen	8.479 ± 0.006	7.260 ± 0.006	—	—	—	—
V0381 Cen	7.675 ± 0.006	6.791 ± 0.006	—	—	—	—
V0386 Cyg	9.624 ± 0.007	—	6.375 ± 0.007	5.809 ± 0.007	5.540 ± 0.015	M11
V0395 Cas	10.748 ± 0.019	9.447 ± 0.035	—	—	—	—
V0402 Cyg	9.864 ± 0.006	—	7.809 ± 0.006	7.416 ± 0.006	7.263 ± 0.015	M11
V0459 Cyg	10.576 ± 0.033	8.881 ± 0.019	7.613 ± 0.011	7.075 ± 0.010	6.859 ± 0.016	M11
V0470 Sco	11.005 ± 0.008	8.246 ± 0.007	—	—	—	—
V0493 Aql	11.046 ± 0.006	—	—	—	—	—
V0496 Aql	7.769 ± 0.006	6.489 ± 0.008	—	—	—	—
V0496 Cen	9.945 ± 0.006	8.539 ± 0.006	—	—	—	—
V0508 Mon	10.502 ± 0.006	9.461 ± 0.006	—	—	—	—
V0520 Cyg	10.852 ± 0.006	9.306 ± 0.029	—	—	—	—
V0538 Cyg	10.449 ± 0.009	8.971 ± 0.049	7.803 ± 0.007	7.311 ± 0.006	7.119 ± 0.008	M11
V0600 Aql	10.034 ± 0.006	8.281 ± 0.011	—	—	—	—
V0609 Cyg	11.026 ± 0.017	8.683 ± 0.015	6.832 ± 0.013	6.128 ± 0.010	5.800 ± 0.017	M11
V0636 Cas	7.183 ± 0.006	—	—	—	—	—
V0636 Sco	6.654 ± 0.006	5.649 ± 0.006	—	—	—	—
V0733 Aql	9.976 ± 0.006	9.040 ± 0.012	—	—	—	—
V0737 Cen	6.724 ± 0.006	5.701 ± 0.006	—	—	—	—
V1154 Cyg	9.186 ± 0.006	8.180 ± 0.018	—	—	—	—
V1162 Aql	7.806 ± 0.006	6.850 ± 0.007	6.143 ± 0.008	5.814 ± 0.017	5.682 ± 0.020	M11
VV Cas	10.768 ± 0.016	9.432 ± 0.018	8.328 ± 0.008	7.885 ± 0.006	7.719 ± 0.008	M11
VW Cen	10.263 ± 0.007	8.783 ± 0.006	7.555 ± 0.007	7.015 ± 0.006	6.775 ± 0.006	L92
VW Cru	9.597 ± 0.009	7.977 ± 0.006	—	—	—	—

Table 5 (continued)

Star	V (mag)	I (mag)	J (mag)	H (mag)	K_S (mag)	Ref. NIR
VW Pup	11.393 ± 0.007	10.091 ± 0.006	—	—	—	—
VY Car	7.460 ± 0.006	6.283 ± 0.006	5.375 ± 0.015	4.943 ± 0.010	4.760 ± 0.010	L92, W84
VY Cyg	9.594 ± 0.006	8.127 ± 0.019	7.009 ± 0.006	6.552 ± 0.009	6.355 ± 0.010	M11
VY Per	11.221 ± 0.014	9.297 ± 0.026	—	—	—	—
VY Sgr	11.469 ± 0.012	9.129 ± 0.013	—	—	—	—
VZ Cyg	8.970 ± 0.008	7.966 ± 0.015	7.201 ± 0.007	6.864 ± 0.006	6.721 ± 0.006	B97, W84, M11
VZ Pup	9.657 ± 0.009	8.302 ± 0.006	7.277 ± 0.007	6.830 ± 0.006	6.626 ± 0.006	L92
W Gem	7.012 ± 0.049	—	5.129 ± 0.033	4.771 ± 0.026	4.656 ± 0.021	M11
W Sgr	4.664 ± 0.006	3.850 ± 0.006	—	—	—	—
WW Car	9.750 ± 0.010	8.644 ± 0.007	—	—	—	—
WW Pup	10.599 ± 0.010	9.525 ± 0.007	—	—	—	—
WX Pup	9.070 ± 0.007	7.968 ± 0.006	—	—	—	—
WY Pup	10.599 ± 0.013	9.662 ± 0.008	—	—	—	—
WZ Pup	10.320 ± 0.006	9.424 ± 0.006	—	—	—	—
WZ Sgr	8.046 ± 0.011	6.544 ± 0.010	5.282 ± 0.008	4.761 ± 0.006	4.538 ± 0.008	L92, W84, M11
X Cru	8.404 ± 0.006	—	—	—	—	—
X Cyg	6.385 ± 0.009	5.236 ± 0.028	4.383 ± 0.008	3.960 ± 0.006	3.799 ± 0.006	W84, B97
X Pup	8.517 ± 0.011	7.161 ± 0.006	6.077 ± 0.023	5.599 ± 0.011	5.386 ± 0.011	L92
X Sct	10.031 ± 0.017	8.613 ± 0.033	—	—	—	—
X Sgr	4.548 ± 0.006	3.652 ± 0.006	2.950 ± 0.007	2.635 ± 0.007	2.505 ± 0.010	F08, W84
X Vul	8.834 ± 0.006	7.198 ± 0.020	5.928 ± 0.010	5.433 ± 0.008	5.214 ± 0.015	M11
XX Cen	7.824 ± 0.006	6.743 ± 0.006	5.914 ± 0.008	5.541 ± 0.006	5.375 ± 0.007	L92, W84
XX Mon	11.914 ± 0.007	10.505 ± 0.009	—	—	—	—
XX Sgr	8.869 ± 0.006	7.506 ± 0.006	6.412 ± 0.033	5.964 ± 0.018	5.799 ± 0.022	W84
XX Vel	10.676 ± 0.006	9.302 ± 0.006	—	—	—	—
XZ Car	8.597 ± 0.006	7.248 ± 0.006	—	—	—	—
Y Aur	9.809 ± 0.044	—	7.660 ± 0.007	7.291 ± 0.008	7.133 ± 0.026	M11
Y Lac	9.159 ± 0.007	8.308 ± 0.026	7.626 ± 0.006	7.316 ± 0.006	7.201 ± 0.008	B97, M11
Y Oph	6.148 ± 0.006	4.533 ± 0.006	3.349 ± 0.006	2.874 ± 0.006	2.662 ± 0.008	W84, L92
Y Sct	—	—	6.472 ± 0.009	5.897 ± 0.011	5.646 ± 0.014	M11
Y Sgr	5.739 ± 0.006	4.790 ± 0.006	—	—	—	—
YZ Aur	10.346 ± 0.009	—	7.498 ± 0.015	6.905 ± 0.011	6.689 ± 0.024	M11
YZ Car	8.714 ± 0.006	7.438 ± 0.006	—	—	—	—
YZ Sgr	7.351 ± 0.006	6.226 ± 0.006	5.379 ± 0.007	5.004 ± 0.009	4.861 ± 0.010	M11, W84
Z Lac	8.417 ± 0.006	7.198 ± 0.043	6.235 ± 0.009	5.811 ± 0.006	5.653 ± 0.008	B97, M11
Z Sct	—	—	6.962 ± 0.017	6.483 ± 0.016	6.282 ± 0.017	M11
ζ Gem	3.889 ± 0.006	3.096 ± 0.006	2.538 ± 0.006	2.210 ± 0.006	2.096 ± 0.006	F08

